LAWRENCE
LIVERMORE
NATIONAL
LABORATORY

UCRL-TH-219069

Two-axis Beam Steering Mirror Control system for Precision Pointing and Tracking Applications

Klaus Ulander

February 16, 2006

Disclaimer

This document was prepared as an account of work sponsored by an agency of the United States Government. Neither the United States Government nor the University of California nor any of their employees, makes any warranty, express or implied, or assumes any legal liability or responsibility for the accuracy, completeness, or usefulness of any information, apparatus, product, or process disclosed, or represents that its use would not infringe privately owned rights. Reference herein to any specific commercial product, process, or service by trade name, trademark, manufacturer, or otherwise, does not necessarily constitute or imply its endorsement, recommendation, or favoring by the United States Government or the University of California. The views and opinions of authors expressed herein do not necessarily state or reflect those of the United States Government or the University of California, and shall not be used for advertising or product endorsement purposes.

This work was performed under the auspices of the U.S. Department of Energy by University of California, Lawrence Livermore National Laboratory under Contract W-7405-Eng-48.

Two-Axis Beam Steering Mirror Control System for Precision Pointing and Tracking Applications

A Thesis
Presented to the Faculty of
California Polytechnic State University
San Luis Obispo

In Partial Fulfillment
Of the Requirements for the Degree
Master of Science in Electrical Engineering

By
Klaus Ulander
Summer 2006

AUTHORIZATION FOR REPRODUCTION

OF MASTER'S THESIS

I grant permission for the reproduction of this thesis in its entirety or any of its parts, without further authorization from me.

_____

Signature (Klaus Ulander)

_____

Date

APPROVAL PAGE

TITLE:
Two-Axis Beam Steering Mirror Control System for Free-Space Optical Communication

AUTHOR:

Klaus Ulander

DATE SUBMITTED:

_____ _____

Dr. Fred W. DePiero, Committee Chair

_____ _____

Dr. C. Art MacCarley, Committee Member

_____ _____

Dr. Xiao-Hua (Helen) Yu, Committee Member

ABSTRACT

Two-Axis Beam Steering Mirror Control System for Precision Pointing and Tracking Applications

Precision pointing and tracking of laser beams is critical in numerous military and industrial applications. This is particularly true for systems requiring atmospheric beam propagation. Such systems are plagued by environmental influences which cause the optical signal to break up and wander. Example applications include laser communications, precision targeting, active imaging, chemical remote sensing, and laser vibrometry. The goal of this project is to build a beam steering system using a two-axis mirror to maintain precise pointing control. Ultimately, position control to 0.08% accuracy (40 μrad) with a bandwidth of 200 Hz is desired. The work described encompasses evaluation of the instrumentation system and the subsequent design and implementation of an analog electronic controller for a two-axis mirror used to steer the beam. The controller operates over a wide temperature range, through multiple mirror resonances, and is independent of specific mirrors. The design was built and successfully fielded in a Lawrence Livermore National Laboratory free-space optics experiment. All measurements and performance parameters are derived from measurements made on actual hardware that was built and field tested. In some cases, specific design details have been omitted that involve proprietary information pertaining to Lawrence Livermore National Laboratory patent positions and claims. These omissions in no way impact the general validity of the work or concepts presented in this thesis.

ACKNOWLEDGEMENTS

I would like to take this opportunity to thank the SATRN Team at Lawrence Livermore National Laboratory for all of their technical insight and generous mentoring. I'd like to extend my gratitude to Dr. Fred DePiero for teaching me to back away from the details and embrace the bigger picture. Many thanks for taking me on time and time again, and guiding me through this final phase of my education. To the Chadillac, for his robust fortitude is razzing me over never completing my thesis… you've got nothing on me now! To my parents, Torben and Lise, who have always taught by example and remain an inspiration for greatness. Many thanks to my brother, Peder, for reminding me it all really is quite silly and we should just enjoy it while we are here. When are we going to rebuild the gate the dog ate? And to Jill, for her understanding, support, and inspirational lack of patience as we navigate this nebulous maze we call life, I can't thank you enough.

LIST OF FIGURES

TABLE OF CONTENTS

1 Background

The purpose of this thesis is to build a beam steering system using a two-axis mirror to maintain precise pointing control for an optical receiver system. The example application is a long range (several kilometers) free space optical communication system. Atmospheric effects cause the beam to wander as it propagates through free space due to thermal gradients. The steering mirror serves to direct the centroid of the incoming beam onto a receiver.

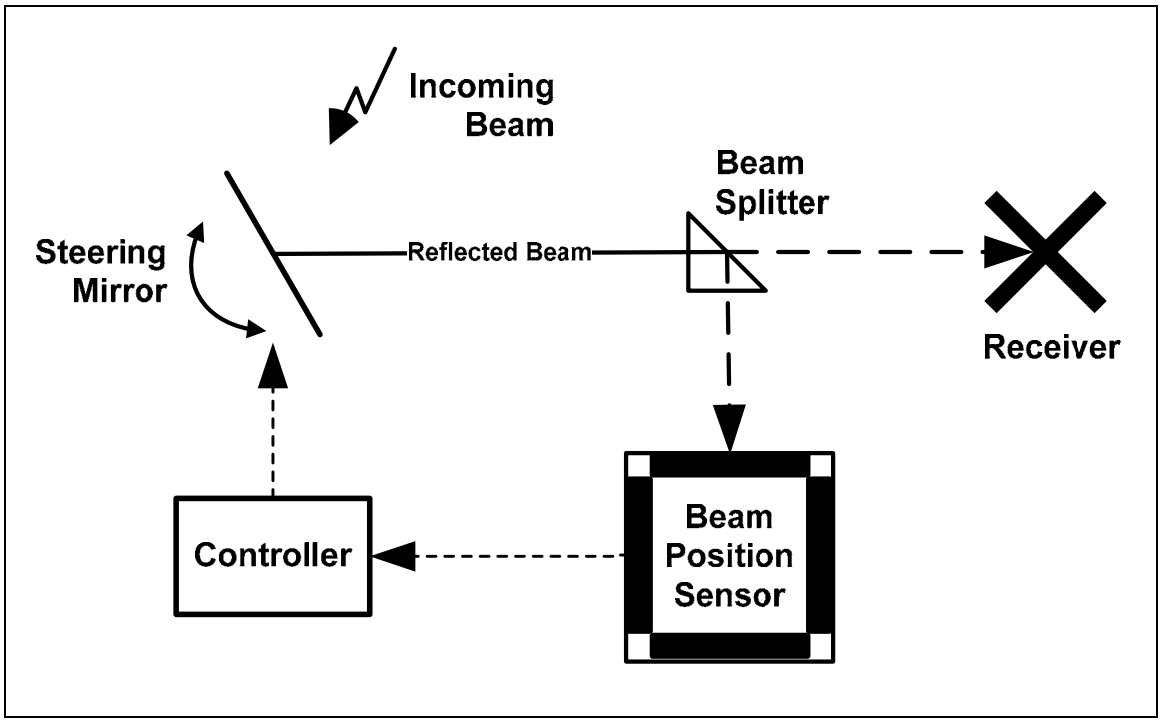

Figure 1 System Overview of Components of a Free Space Optical Communications Receiver

Figure 1 shows a simple overview of a laser communications system. A laser beam arrives through the input aperture of an optics package. The beam is reflected off a movable steering mirror and passes through a beam splitter. The beam splitter directs most of the beam energy on to the target receiver (typically a fiber), and directs a portion

of the beam on to a beam position sensor. The beam sensor and receiver are bore-sighted and virtually in identical locations, meaning a 5 micron motion on the position sensor is equivalent to a 5 micron motion on the receiver. The beam sensor converts optical energy into electrical signals that can be used to determine the position of the beam on the sensor. These signals are used to control the mirror to steer the beam to the center of the beam sensor, and consequently the center of the receiver, thereby compensating for beam drift and wander through the atmosphere.

Project Management dictated an analog solution would be the first step in an iterative approach to designing an optimal controller. This decision was made to allow for rapid prototyping of a deployable system while still defining the plant model so vital to a robust controller design.

All measurements and performance parameters are derived from measurements made on actual hardware that was built and field tested. In some cases, specific design details have been omitted that involve proprietary information pertaining to Lawrence Livermore National Laboratory patent positions and claims. These omissions in no way impact the general validity of the work or concepts presented in this thesis.

2 System Description

The plant under inspection is a commercially available two-axis steering mirror assembly, with a 9 mm diameter and 50 mrad tip/tilt range. Packed within its Titanium casing are two pairs of low voltage piezo-ceramic stack actuators that push and pull the mirror around two orthogonal axes. Linked to the mirror are strain gauges, configured as a full bridge, which provide position feedback signals. A 5 mm diameter Position Sensitive Detector (PSD) monitors the incoming beam. The PSD is virtually in the same location as the fiber due to the optical setup. Along with the strain gauges, the PSD provides the error signal to steer the mirror. Ultimately, the piezo-ceramic transducers are the devices that require precise control. **Figure 2** illustrates the basic block diagram.

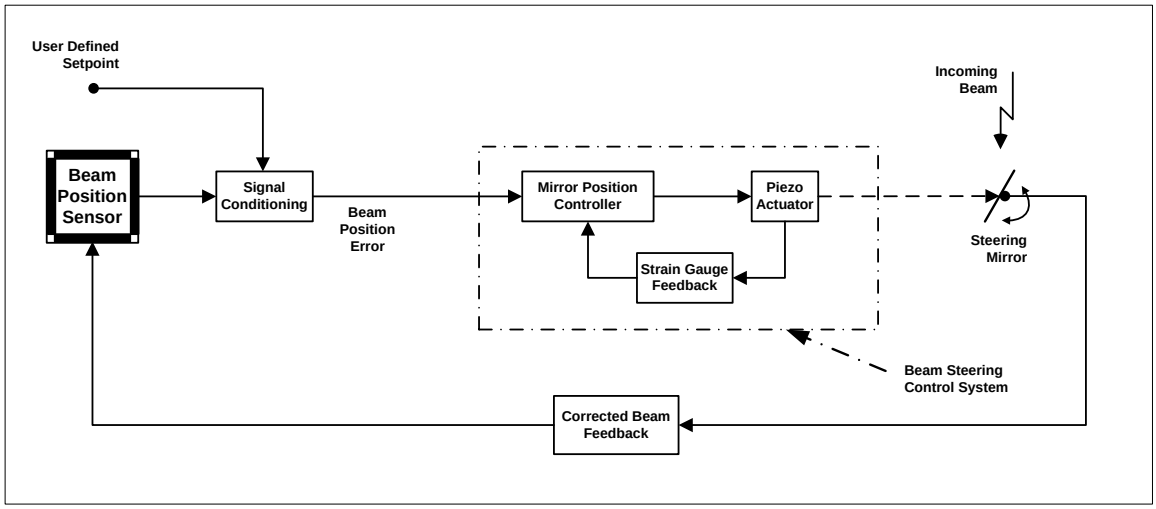

Figure 2 Basic Block Diagram

2.1 Design Goals

The design goal of this project is to replace an existing benchtop mirror controller with a more versatile controller. Specific goals are to reach a bandwidth of 200 Hz,

maintain pointing accuracy to 0.08% of full scale, and operation over a 55°C temperature range. Each benchtop controller is matched and calibrated to a specific mirror at room temperature. Providing a controller that is independent of specific mirrors is desirable. Bandwidth shall be characterized both with the standard 3dB criteria, as well as the point at which a 45° phase shift occurs.

2.2 Major Components

2.2.1 Position Sensitive Detector

A 5 mm diameter tetra-lateral Position Sensitive Detector (PSD) is used, along with a computer supplied setpoint command, to provide the control signal for steering the mirror. Due to the optical properties and precision alignment of the optical setup, the PSD is optically in the same location as the target on which the light must be maintained. (Refer to **Figure 1**.) By steering the incoming beam to the center of the PSD, the beam will also be centered on the target.

2.2.1.1 PSD Basics

A PSD is the analog equivalent of a Charge Coupled Device (CCD). Essentially, it is a PIN photodiode with a resistive P-layer. An incident beam of light causes an electric potential to generate photocurrents at each of its four electrodes due to the photovoltaic effect (**See Figure 3**).

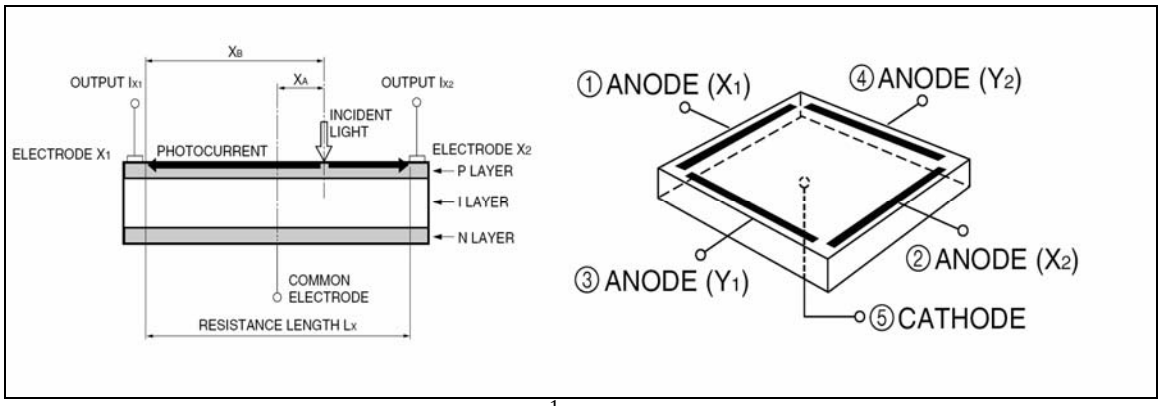

Figure 3 Conceptual Drawing of PSD Structure [1]

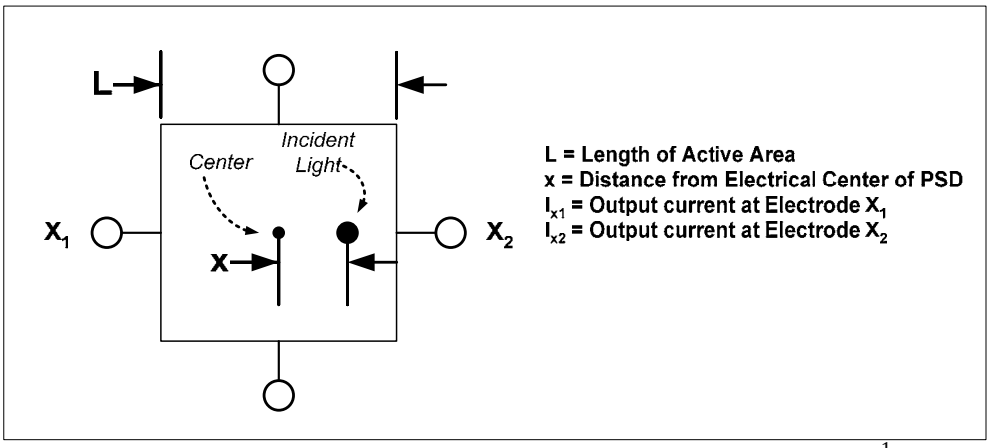

Figure 4 Calculation of Position of Incoming Beam is Based on PSD Currents[1]

The currents are used to determine the centroid of the incident light hitting the device in each axis based on the **Figure 4** and the formula below[1]:

$$X = \frac{L}{2} \times \frac{(I_{x2} - I_{x1})}{(I_{x2} + I_{x1})}, \quad \text{similarly, for the y-axis: } Y = \frac{L}{2} \times \frac{(I_{y2} - I_{y1})}{(I_{y2} + I_{y1})}$$

2.2.2 Piezo-ceramic Actuators

Piezoelectric materials build up electrical charges when physically compressed, due to a property known as the piezo-electric effect. Conversely, when exposed to electric fields, these materials expand.[2] This induced force due to an electric charge is known as the Inverse Piezoelectric Effect. These materials are known to exhibit non-

linear behaviour in the form of hysteresis. Goldfarb and Celanovic[3] conducted notable research and employed a derivation from the Maxwell slip model for modeling the piezoelectric actuator with hysteresis.

Actual displacement of the material is minute (anywhere from 10s of picometers to 100s of microns[4]); however if several slices of piezoceramic wafers are stacked mechanically in series, and electrically connected in parallel to a stimulation source, the displacement can be amplified (to 10's of millimeters). **Figure 5** below shows the concept of a piston-motion piezoceramic actuator.

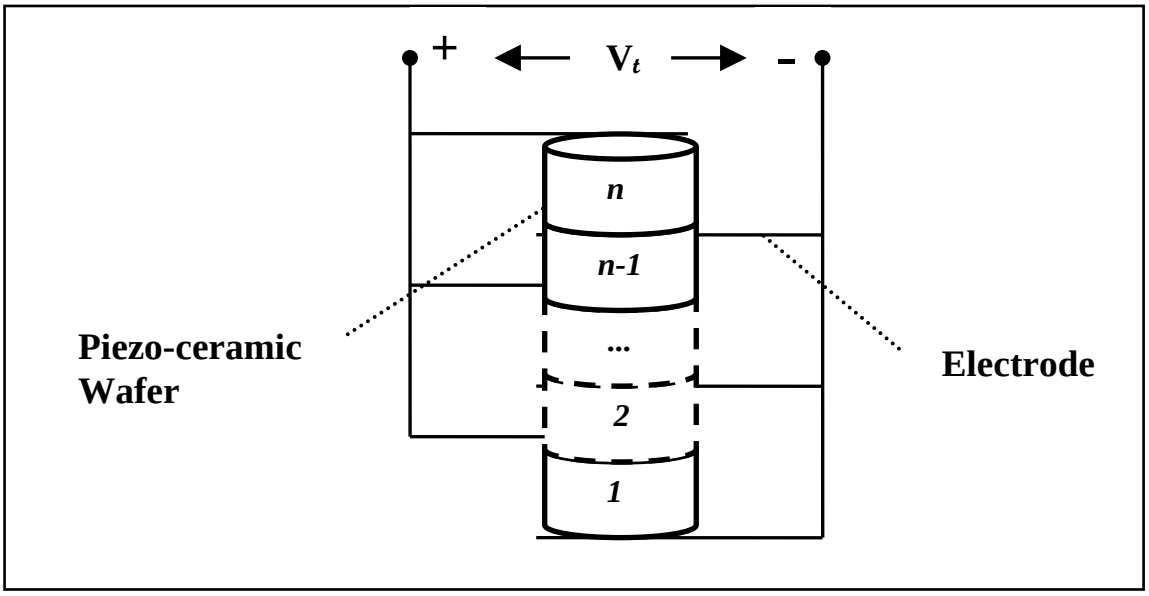

Figure 5 Conceptual Sketch of a Piezoelectric Stack Actuator

2.2.2.1 Application of the PZT Actuator to Steer the Mirror

Figure 6 below illustrates the electromechanical concept of how the piezo-ceramic actuators steer the mirror. Each axis of the mirror is steered using two piezo-ceramic transducer (PZT) stack actuators that work in combination to push or pull the mirror around the axis. The PZTs are connected in series. One side of "PZT X2" is

connected to a 100V reference channel (***Node 3***), while the opposite side of "PZT X1" is connected to a ground reference (***Node 4***). An active channel, with a range of 0-100V, is connected to the common point between the two PZTs (***Node 1***). As the voltage of the active channel increases, one PZT expands while the other PZT contracts, and vice versa for decreasing voltage. This scheme is duplicated for the Y-Axis. Total motion is ±25 mrad, or approximately ±1.43°.

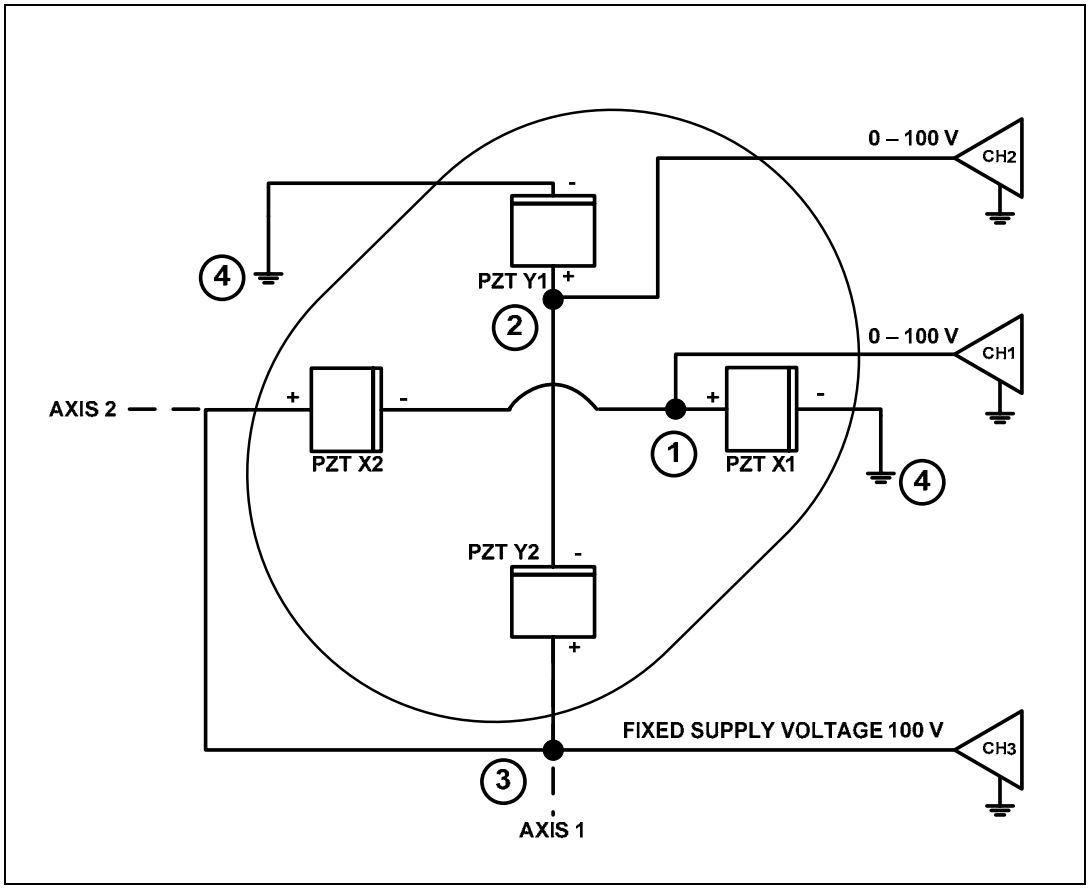

Figure 6 PZT Actuator Conceptual Drawing

2.2.3 Strain Gauges

As mentioned previously, the mirror is linked to strain gauges that report mirror position information. A strain gauge, in effect, is a resistive element that varies its resistance as it is stressed or strained. In fact, what occurs to the gauge as it is stressed is a change in its length and cross-sectional area, which in turn changes the resistance of the gauge[5]. When given a voltage reference in a bridge circuit, this change in resistance results in a difference in voltage across the bridge. Although the difference it quite small, it is this difference that indicates how the mechanical component under observation is moving or deforming. Properly measuring this differential signal, with care toward common mode suppression and noise minimization can allow for precise monitoring of the mechanical component.

2.2.3.1 The Strain Gauge Bridge

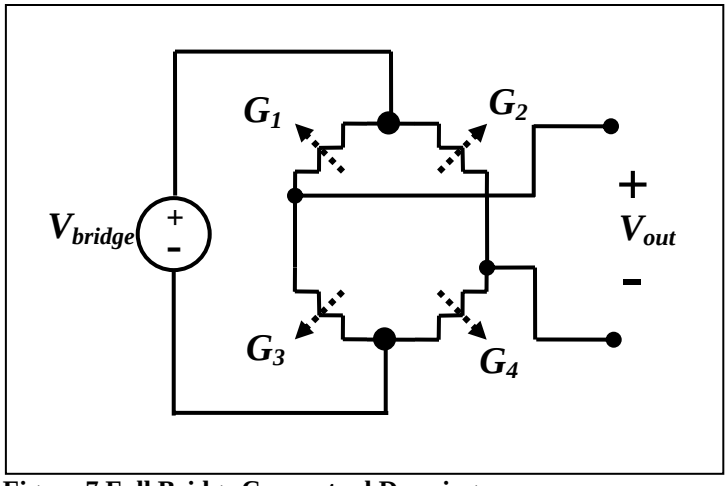

Figure 7 Full Bridge Conceptual Drawing

The gauges in the steering mirror are arranged in a full bridge. **Figure 7** depicts a full bridge, the optimum configuration from a thermal perspective. As the temperatures rise, the gauges expand. As the gauges expand and contract together, a common mode

effect is created that can be eliminated with proper circuitry. In fact, the bridge circuit is designed to reject common mode and measure a differential mode signal. For example, in **Figure 7**, if strain gauges G1 and G2 expand at the same rate, there will be shift in the center of the bridge referenced to $\boldsymbol{V_{bridge}}$, yet $\boldsymbol{V_{out}}$ is immune to the change. Similarly, if all gauges G1, G2, G3, and G4 have an equal decrease in resistance, $\boldsymbol{V_{out}}$ will not observe any change. However, if G1 experiences a mechanical stress causing its resistance value to change while G2 stays constant, the bridge will become unbalanced, and a voltage will be observed at $\boldsymbol{V_{out}}$. This is precisely the advantage of using the bridge to measure mechanical stress and strain.

3 Sensor Characterization

A clear understanding of each sensor and how they operate is necessary before design of a controller can begin. The following chapter examines the piezo-ceramic transducers, strain gauges, and PSD and defines details that must be incorporated into the controller.

3.1 Characterization of Piezo-ceramic Actuators

Sometimes engineers must go through indirect methods to extrapolate information from the systems they are involved with. Such is the case for determining characteristics of the PZTs. Access to these devices to observe their behaviours directly would require destruction of the mirror itself. However, using the optical properties of the mirror under control of the PZTs can yield the information required. Specifically, directing a beam onto the steering mirror, and observing the deflection resulting from discrete changes in the mirror commands can yield the physical behaviour of the PZTs. This method, as depicted in **Figure 8**, was used to determine the linearity of the PZTs. Marking where the beam hits on the wall and using simple trigonometry, the characteristics of the PZTs may be observed. Results obtained had an error or ±250 µrad, or 0.5%.

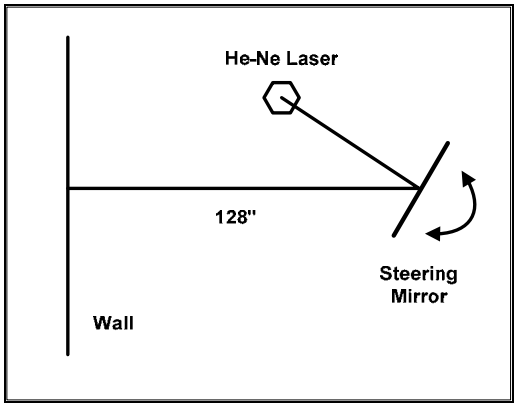

Figure 8 PZT Characterization Test Setup

The results of that experiment are displayed in the graph depicted in **Figure 9**. What is observed is a classic example of non-linear behaviour in the form of hysteresis.

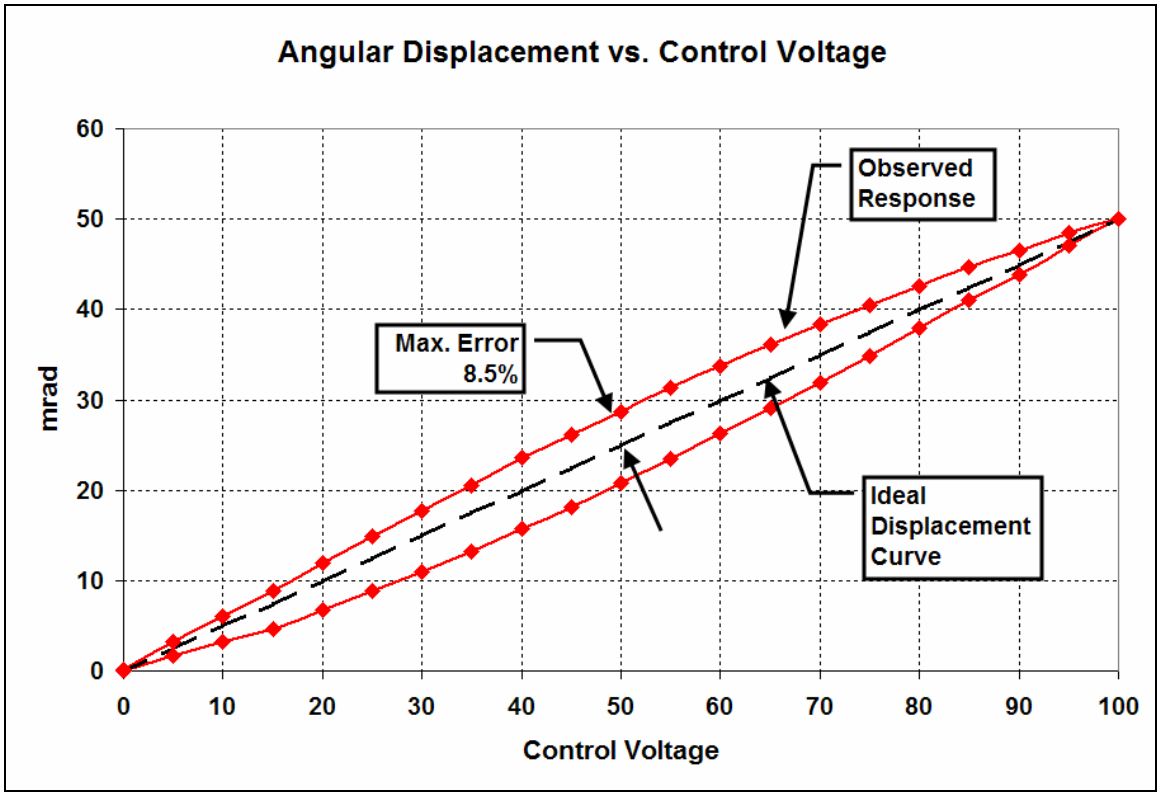

Figure 9 Exhibited Hysteresis in PZT

The angular displacement of the mirror does not correspond directly with the command voltage. It is dependent upon which direction the motion of the mirror is, which indicates that an open loop controller with simply a command voltage will not suffice to maintain precise position control.

3.2 Characterization of Strain Gauges

3.2.1 Strain Gauge Linearity

A similar test was performed to determine the response of the strain gauges. An amplifier was used to supply the reference and drive signals to steer the mirror to discrete locations. The microvolt signals generated by the imbalance in the strain gauge bridge were amplified using a low noise instrumentation amplifier and read from a digital voltmeter. Angular measurements had a 0.5% margin of error. The results are displayed in **Figure 10**.

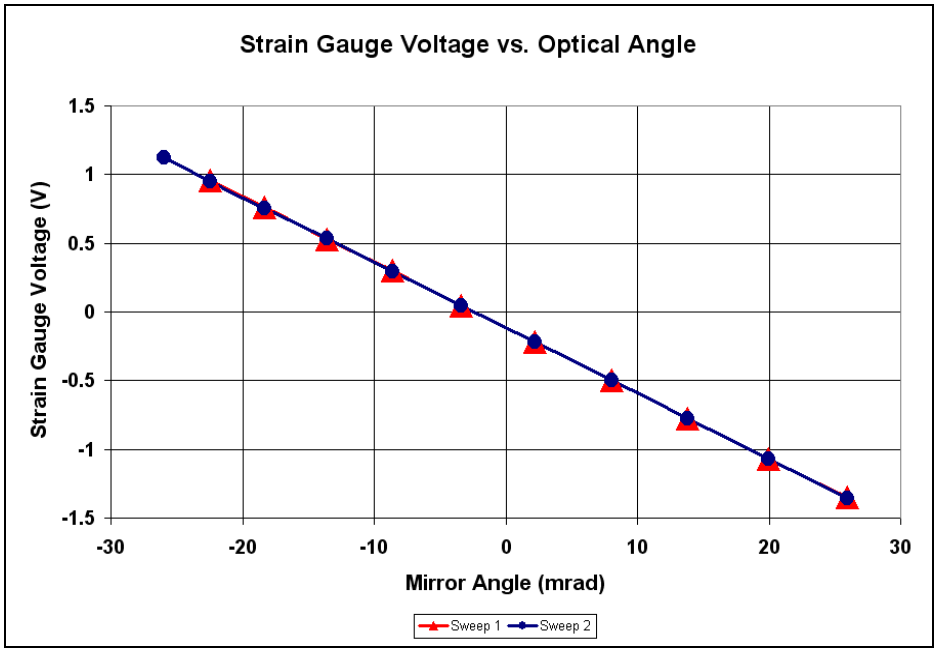

Figure 10 Strain Gauge Linearity and Repeatability

The observed response is linear and repeatable. This behaviour indicates that the signals generated by the strain gauge bridge will provide accurate positional information which can be used to counteract the hysteresis observed in the PZTs.

3.2.2 Strain Gauge DC Offsets

Further investigation into the behaviour of the strain gauges revealed some variability between steering mirrors, and even between axes on a single mirror. **Figure 11** shows that the slope of the response for the strain gauges remains constant, however offset errors are apparent. Delving into the specifications for the specific strain gauge used in the mirror revealed an expected ±0.2% offset specification. This limit is placed on the graph for reference. An offset adjustment must be incorporated into the design to allow for calibration of individual mirror responses.

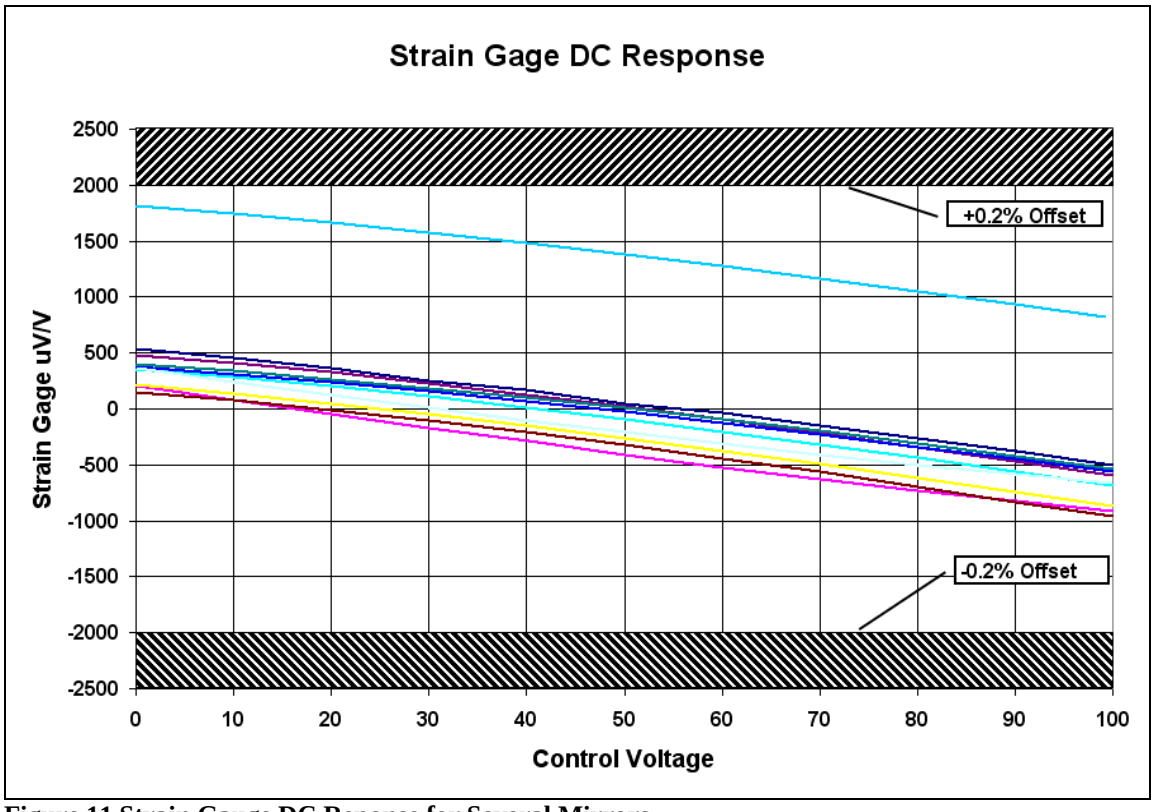

Figure 11 Strain Gauge DC Reponse for Several Mirrors

3.3 Characterization of Position Sensitive Detector

3.3.1 Linearity of PSD

To test the linearity of the PSD, a simple setup was built on an optical breadboard. See **Figure 12**. A laser pumped a beam into a fiber connected to a launch fixture mounted on a translation stage. The beam is pointed at the PSD and each of the four currents is converted to voltage using a simple transimpedance amp configuration of a low noise op-amp. The voltages were monitored with a digitizer and converted to positional data using software to perform the calculations discussed with **Figure 4**. The fiber was moved in discrete steps and measured position recorded. The test setup and results are displayed in **Figures 12 and 13.** Position measurements had a 0.1% error.

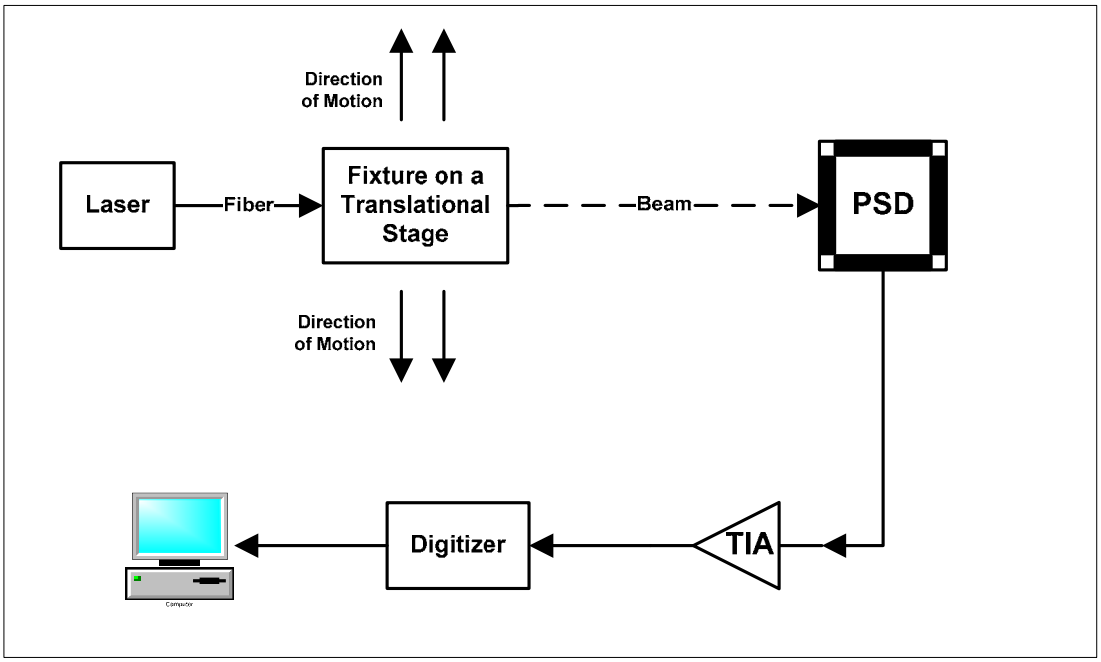

Figure 12 PSD Linearity Test Setup

The slight S-curve of **Figure 13** reveals some non-linearity in the PSD's ability to resolve position. Fortunately, this non-linearity is of little consequence because the saving grace is the intention to keep the centroid of the beam focused on the center of the fiber, which is optically in the identical position. Null detection, system operation generally at the center of the PSD, is the intent of the control scheme, and so the non-linearity can effectively be ignored.

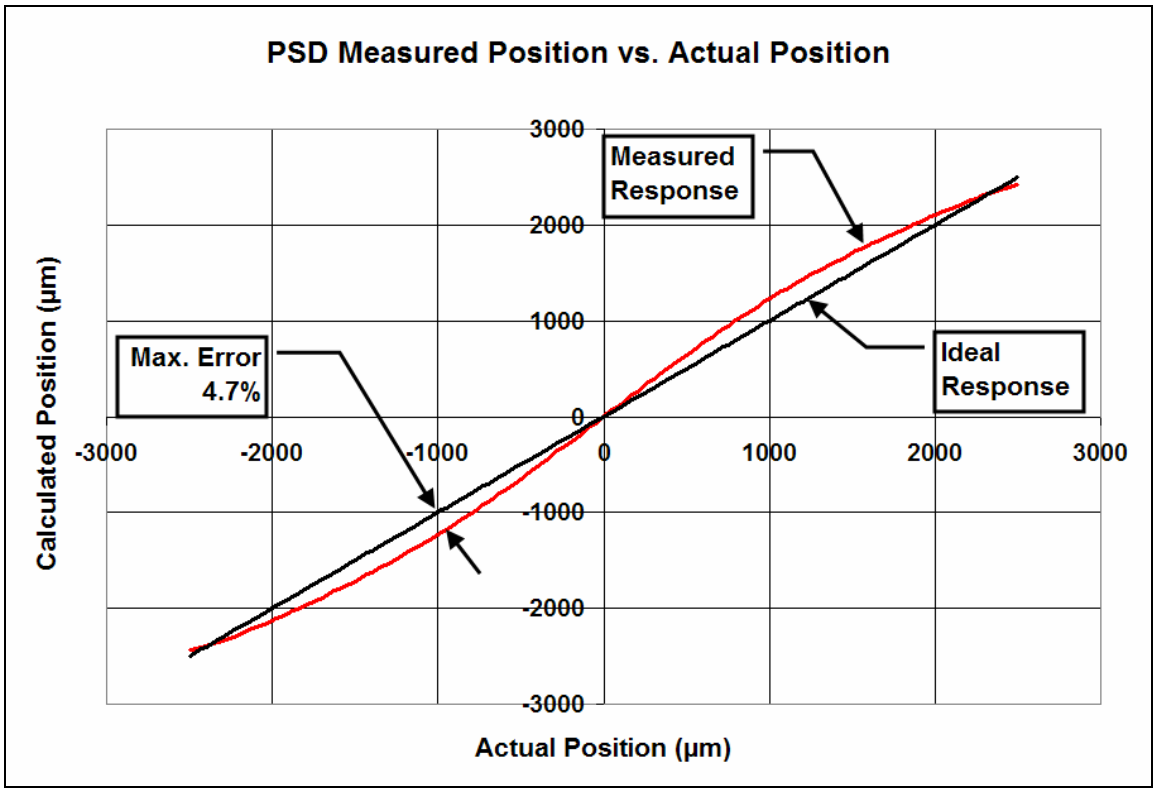

Figure 13 PSD Observed Response

3.3.2 Temperature Drift of PSD

Drift is a common problem in optoelectronic applications. Although the optical setup is beyond the scope of this thesis, the electronics involved are not. Drift in the electronics must be understood to build a controller capable of overcoming that drift. A simple measurement to examine drift of the PSD was performed. The PSD was placed in an environmental chamber with a fiber pointed directly at it. Once again the output of each channel of the PSD was digitized. Logging durations of 10 minutes per temperature setting were used to calculate the average perceived position at that temperature setting. The results of that experiment are shown in **Figure 14** below.

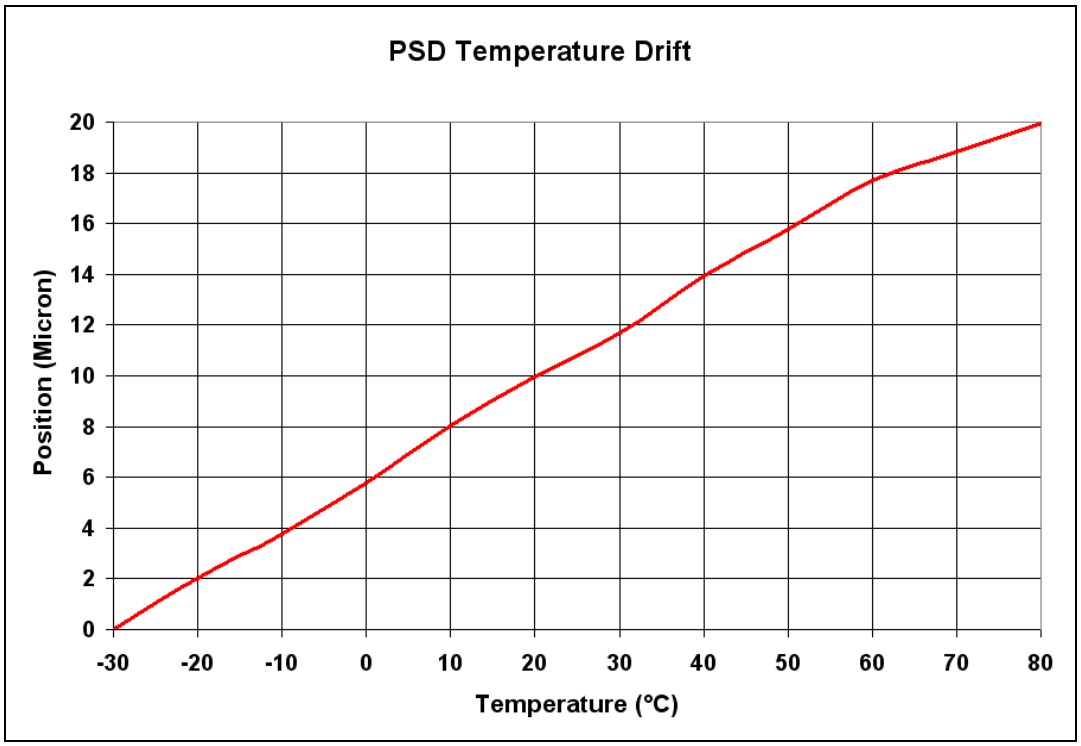

Figure 14 PSD Drift Measurements

The experiment reveals a relatively linear temperature drift of 0.2 micron/°C, or 36 ppm/°C. The intended operating range is from +25ºC to +80ºC. The drift contributed by the PSD will result in a 0.2% error.

$$\underline{\underline{PSD\ Error\ Due\ to\ PSD}} = \frac{(Measured\ PSD\ Drift)(Operating\ Temp\ Range)}{(PSD\ Length)} \times 100\%$$

$$= \left(\frac{0.2\ micron}{°C}\right)\left(\frac{55°C}{5{,}000\ micron}\right) \times 100\%$$

$$= \underline{\underline{0.2\%}}$$

4 Open Loop System Dynamic Response

The dynamic response of the system, as a whole, is also important to characterize. Careful analysis of these dynamics reveals information that can be used to build a model of the plant. Often the step response is used in linear time invariant systems to determine model characteristics. As we have observed, the system has inherent hysteresis, which of course eliminates the time invariant status of the system. However, the step response, along with the aid of computer models and estimators, can indeed still be used to develop higher order models that account for non-linearities such as hysteresis and resonance. The frequency response of the system can still yield a great deal of information. This was the primary form of initial system analysis used to determine system characteristics.

4.1 Frequency Response

To examine the frequency response, a Vector Signal Analyzer (VSA) was used to inject a small, white noise signal on the command signal to the mirror. This noise signal was fed into one input of the VSA and the feedback from the strain gauge bridge was fed into the other channel. The VSA produced the results of the transfer function.

$$VSA\ Output = \frac{System\ Output}{System\ Input} = \frac{Y(s)}{R(s)} = G(s) = \text{System Transfer Function}$$

Figure 15 below shows the frequency response of the mirror.

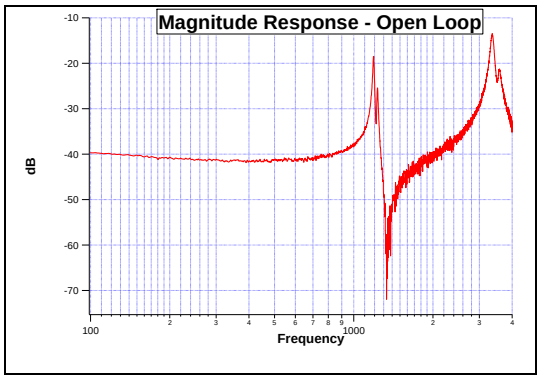

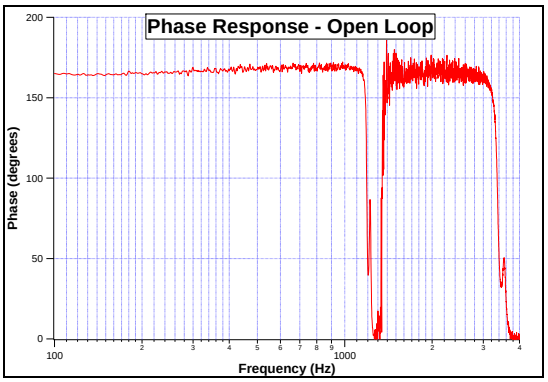

Figure 15 Frequency Response of Mirror

What is observed is the mirror appears to have two resonances. The first resonance occurs roughly at 1.1 kHz, and the second resonance at roughly 2.9 kHz. The phase is relatively flat until the first resonance, where it takes decreases rapidly. The effects of the resonance on the magnitude response appears at a lower frequency than the effects to the phase, and so the magnitude response appears to be of greater concern. A simple solution to this issue of resonance is to simply implement a low pass filter to prevent operation close to these frequencies. However, the goal of the project is to build an amplifier that moves the steering mirror as fast as possible. Implementing notch filters will counteract the system resonances without sacrificing excessive bandwidth. Implementing filters, however, introduces phase shift and so a balance between speed and phase shift must be found. This topic is discussed in further detail in **Chapter 5**.

Delving further into the frequency response, reveals a bleaker picture. Repeating the experiment for several mirrors reveals that each mirror resonates at different frequencies. An overlay of magnitude responses for various mirrors is displayed in **Figure 16a**. Performing the same experiments over temperature demonstrated the resonances shift in frequency as the operating temperature changes. The experiments were performed as described above, only the steering mirror sat inside an environmental

chamber. **Figure 16b** shows an overlay of responses for a single mirror over temperature. Although not entirely unexpected, it makes the solution to the problem a little trickier.

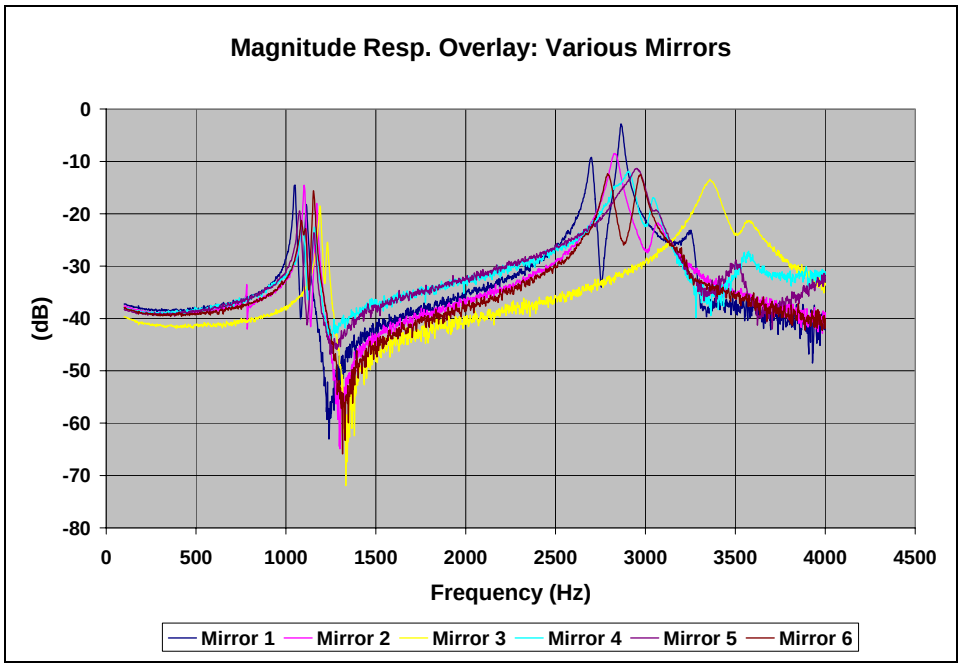

Figure 16a Magnitude Response of Various Mirrors

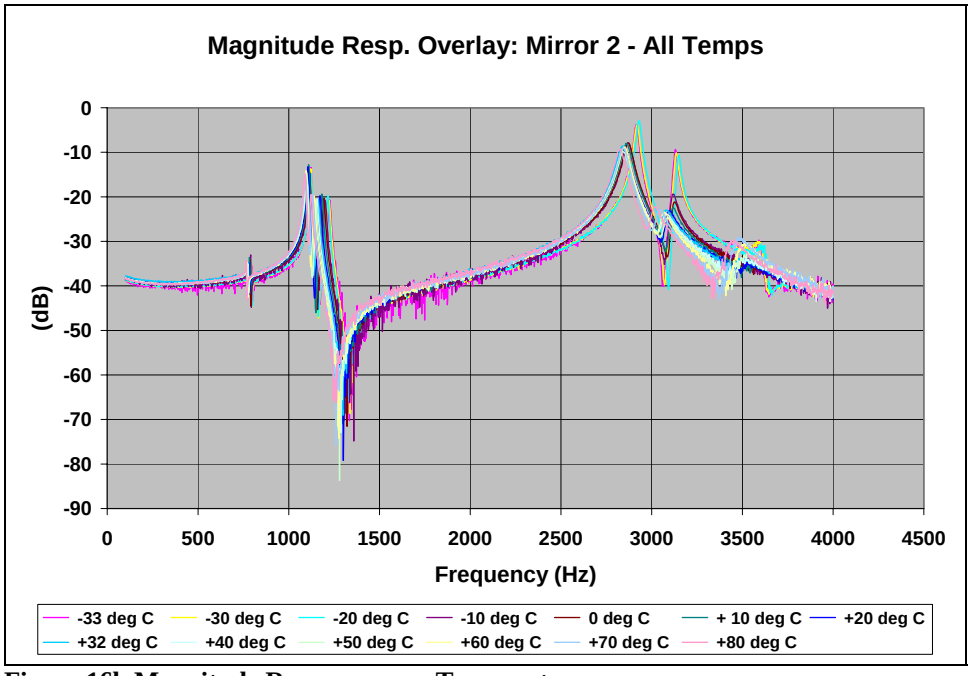

Figure 16b Magnitude Response over Temperature

5 Analog Controller Design

This chapter discusses the controller design. It begins with a review of requirements and design issues, and immediately flows to the control topology selected. Details of each subcomponent and how it is applied to the design are then discussed. Finally, a summary unites the subcomponents into the overall system design displayed in **Figure 17**.

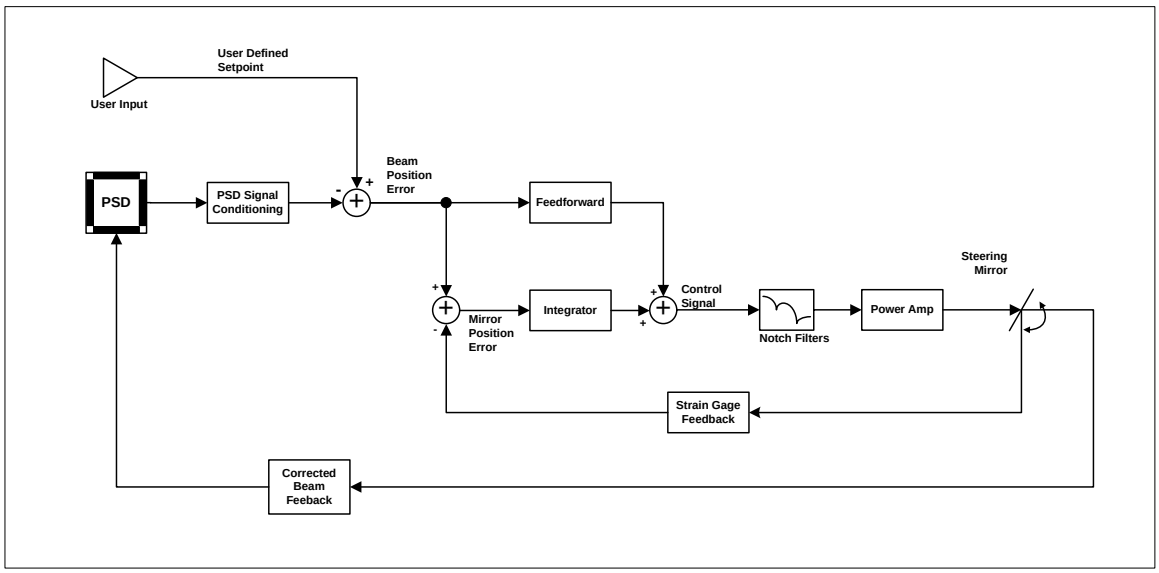

Figure 17 Control Loop Block Diagram

An analog controller is built to steer the mirror. See **Figure 17**. The controller must drive one 100V reference signal and to two 0-100V control signals down a long cable to a capacitive load, namely the PZTs. The microvolt signals generated by the full strain gauge bridges must be scaled to provide feedback signals to the controller. The PSD currents must be converted and scaled appropriately to produce error signals to drive the control loop. The control loop must operate at roughly 200Hz with a pointing accuracy of 40µrad. Setpoints and offsets must be made available to an external user.

Noise and drift must be addressed to maximize pointing accuracy. And finally, care must be taken to avoid exciting the mirror at resonant frequencies of roughly 1.1 kHz and 2.8 kHz. All components used have wide operating temperature ranges with low drift to ensure proper operation over temperature.

5.1 Control Loop –Proportional Integral with Feedforward

The mirror control system presented is a subset of a larger control system. Project management primarily was focused on bandwidth as the parameter to design to. The typical 3dB point is one parameter used to determine bandwidth. Concern over phase contribution to the overall system led to the 45° phase shift point as another bandwidth determining parameter. With that mindset, several control topologies were explored and prototyped to push the bandwidth of the controller out as far as possible.

Variations on phase-lag and phase lead compensations were considered. The Proportional Integral (PI) controller offered low steady state error but exhibited limited bandwidth. A Proportional Derivative (PD) controller showed promise with system bandwidth, however, a reasonable steady state error was hard to achieve.

A variation of the PI controller is selected as the final control topology. The simple Proportional Integral controller once again offers low steady state error. However, the subtle addition of a high-passed feedforward mechanism for the setpoint enables an increase in system bandwidth. The feedforward mechanism seems similar to the derivative term of a PID controller, however it only takes into account changes in the setpoint and ignores process induced changes (i.e. Strain gauge signals). The benefit is response time near that of open loop operation with the accuracy of a closed loop system. **Figure 18** shows the realization of the PI with Feedforward control for the steering

mirror system. It is a simple, yet elegant solution to a high speed precision control problem.

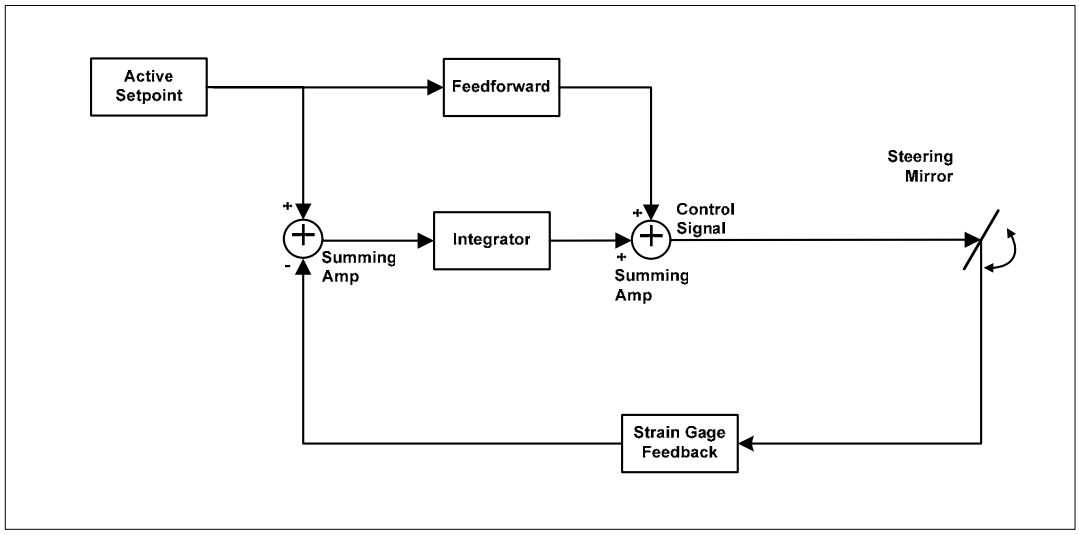

Figure 18 Single Axis PI with Feedforward Control Loop Realization (no output signal conditioning)

5.2 Application of PSD to Steering Mirror System

Recall the currents generated in the PSD from an incoming beam are used to determine the centroid of the incident light hitting the device in each axis based on **Figure 19** and the formula below:

$$X = \frac{L}{2} \times \frac{(I_{x2} - I_{x1})}{(I_{x2} + I_{x1})}, \quad \text{similarly, for the y-axis: } Y = \frac{L}{2} \times \frac{(I_{y2} - I_{y1})}{(I_{y2} + I_{y1})}$$

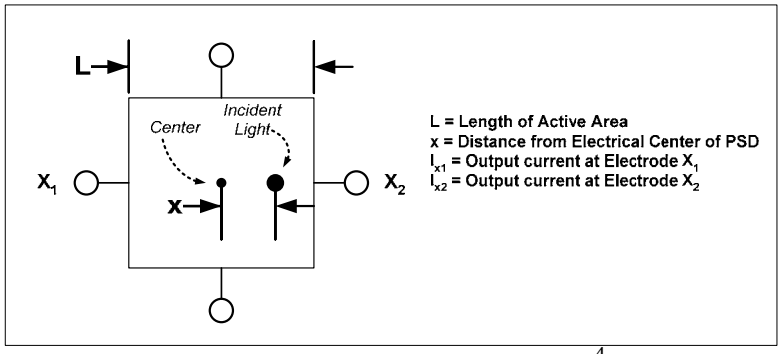

Figure 19 Calculation of Position of Incoming Beam[4]

The difference between resolved PSD position (i.e. X or Y) and the user-defined setpoint generates an error signal to an integrator which generates the "active" setpoint to the mirror controller. The realization of this concept is shown in the block diagram of **Figure 20**.

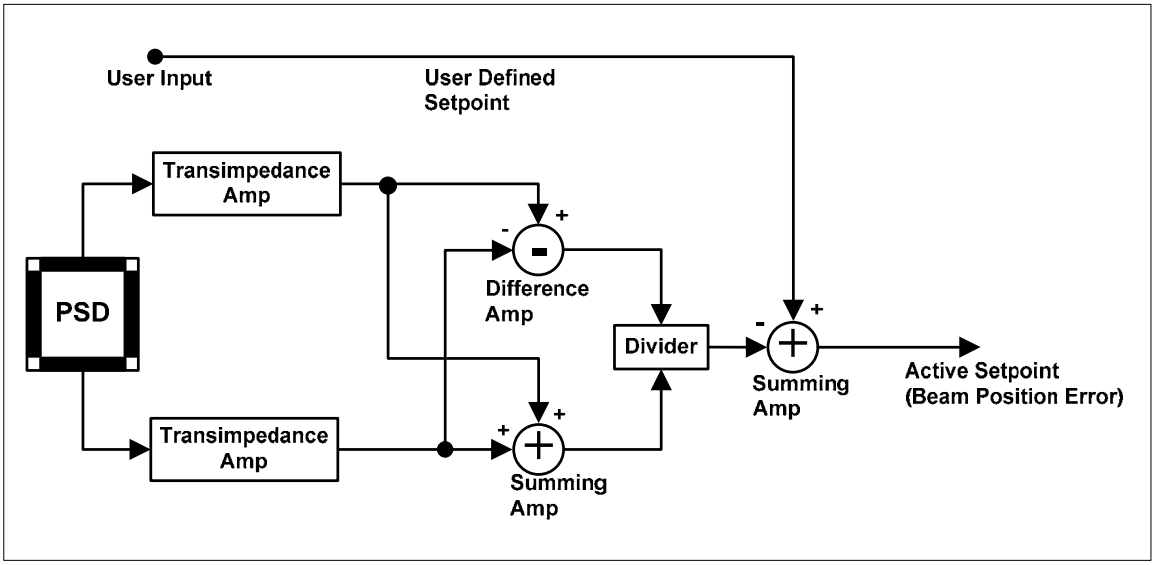

Figure 20 Front End Block Diagram for a Single Axis

The PSD currents must be transformed into voltages and scaled appropriately. This is accomplished with a Transimpedance Amplifier (TIA). To perform the position calculation, summing and difference amplifiers act on the voltages to define the numerator and denominator of the equation. An analog divider performs the calculation to determine the position. And a summing amplifier allows a user to dial in a desired offset. The resulting value is the active setpoint for the controller.

5.3 Application of the Strain Gauge Bridge Amplifier

A full bridge exists for each axis in the steering mirror. Ideally, when the mirror is commanded to its midpoint with a 50V signal, the bridge is balanced and $V_{differential}$ indicates zero volts. As the mirror is commanded away from its midpoint, stresses are applied to the gauges causing their resistance to change, consequently causing the bridge to become unbalanced. When the mirror is commanded to its full range in one direction (i.e. 100V command signal), the bridge will be at its peak imbalance (i.e. $V_{differential} = V_{diff\text{-}max}$); conversely when it is commanded to its full range in the opposite direction (i.e. 0V), the bridge will be at its peak imbalance of opposite polarity (i.e. $V_{differential} = -V_{diff\text{-}max}$). The imbalance range can be scaled to provide position feedback for the controller.

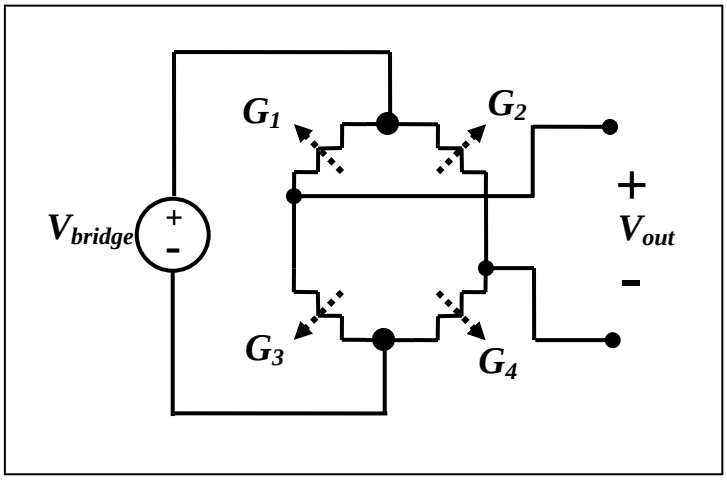

Figure 21 Full Bridge Example

5.3.1 Strain Gauge Bridge Amplifier Design Concepts

The differential signal generated by the imbalance of the strain gauges bridge must be scaled to the "active" setpoint mentioned above. Care must be taken to avoid noise being generated or coupled into these microvolt signals. Over the years, several circuits

have been developed to accurately monitor such signals. One novel approach, presented by Williams[6] (see **Figure 22**) takes advantage of an op-amp to servo the one leg of the bridge at ground. Effectively the final op-amp in the circuit takes a single ended measurement of the differential signal. This method of measurement suppresses common mode effects, and generates low noise signals.

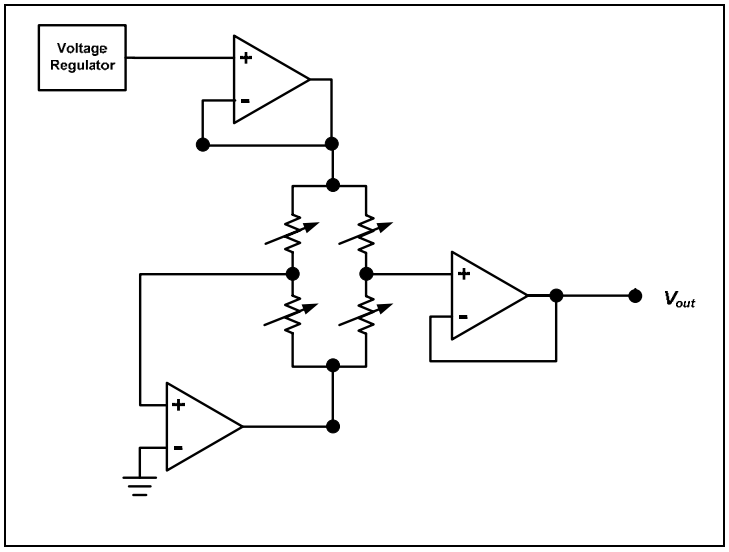

Figure 22 Bridge Circuit with Common Mode Suppression

5.3.2 Practical Considerations for Microvolt Signals

The Strain Gauge Bridge Amplifier is placed as close as possible to the steering mirror to reduce noise coupling and signal loss. The use of guard rings on the circuit board around microvolt signals until they are amplified is another noise reduction technique. A low noise op-amp is employed for amplification. Finally the scaled signal must pass down a long cable, so the last component the signal passes through is a differential driver, to avoid any ground affects.

5.4 Filters

Before the control signal is passed to the mirror some signal conditioning must occur; namely, filtering and scaling the signal to the necessary high voltage levels for the PZTs.

Recall from earlier discussion, the mirror has two known resonances located at roughly 1.1 kHz and 2.8 kHz. What is also known is the resonances vary between mirrors and over temperature. A low pass filter is one simple method to use so that the system would have no chance of exciting the mirror at either of the resonances. That approach would compromise bandwidth, and consequently the choice of implementing two notch filters in an attempt to push the bandwidth out as far as possible was made.

One design goal is to build a controller that will work with all similar steering mirrors, so the notch filters have to be wide enough to accommodate every situation. Open loop response data was taken and folded into computer simulation to examine how the notch filters should be implemented. An iterative approach of varying the center frequency and Q of each filter and applying it to the data was used until a satisfactory predicted response was produced. The basic transfer function for each notch filter[7] is:

$$H(f) = \frac{1 - \left(\frac{f}{f_0}\right)^2}{1 - \left(\frac{f}{f_0}\right)^2 + \frac{j}{Q}\left(\frac{f}{f_0}\right)}$$

The raw, proposed filter, and corresponding filtered simulated responses are illustrated in **Figures 23 and 24** below.

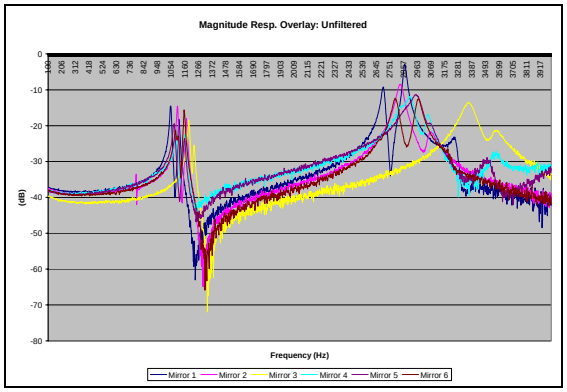

Figure 23a Raw Response - Multiple Mirrors

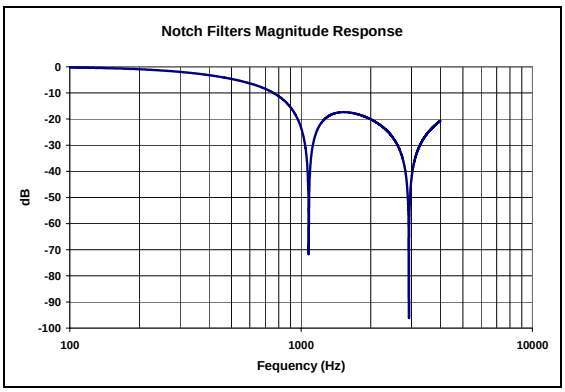

Figure 23b Proposed Filters – Multiple Mirrors

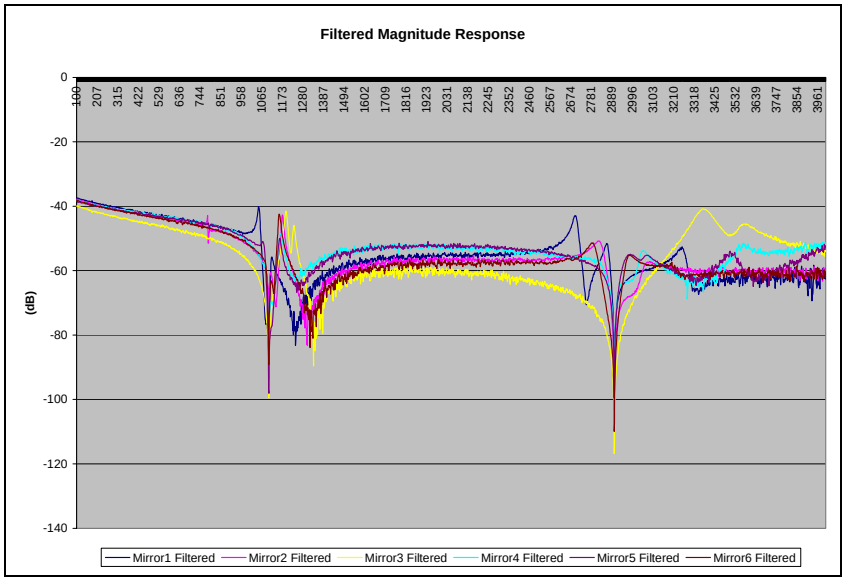

Figure 23c Simulated Response – Multiple Mirrors

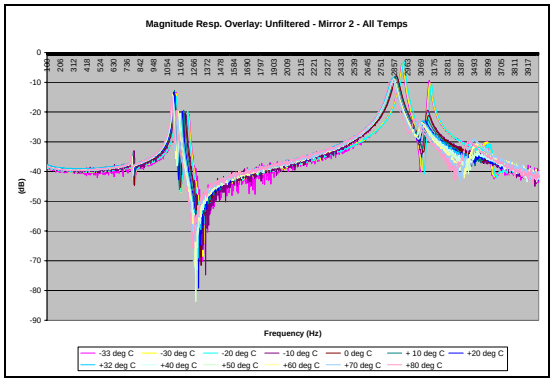

Figure 24a Raw Response - Multiple Temperatures

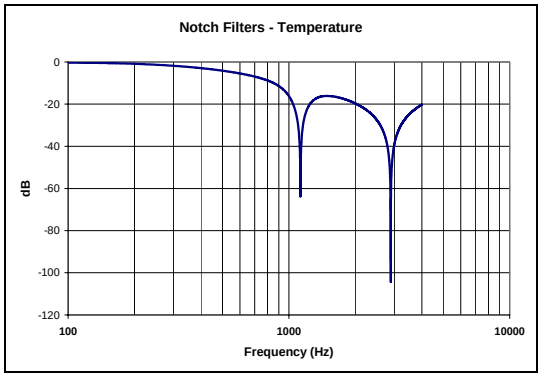

Figure 24b Proposed Filters – Multiple Temp.

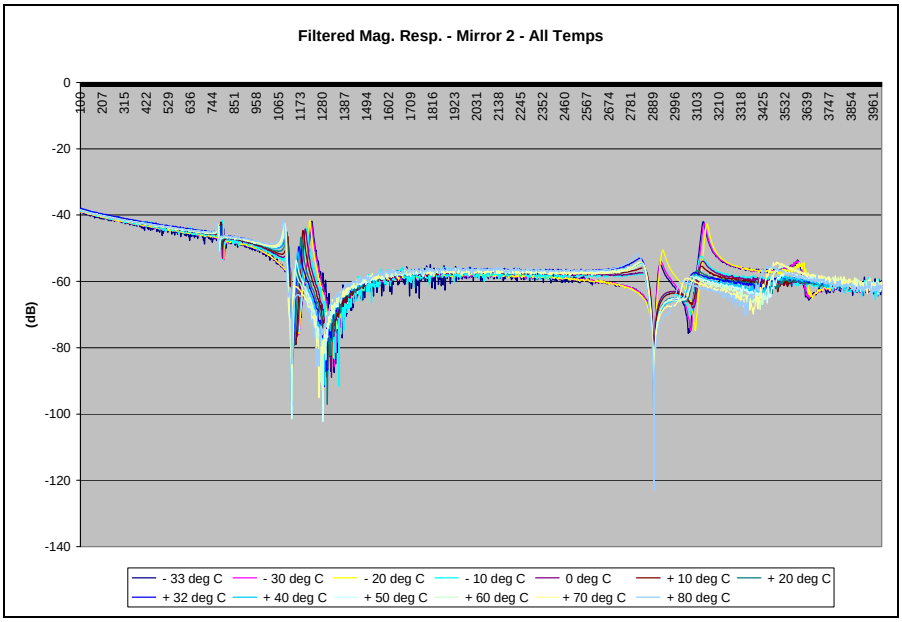

Figure 24c Simulated Response - Multiple Temperatures

5.5 Power Amplifier

The final block in the controller is the output driver for the mirror. A number of published papers offer the use of charge, rather than voltage, to drive the PZTs[1,2,3]. The strain gauges however offer a deterministic position signal, and can be used to counteract the hysteresis of the PZTs. With this in mind, the controller was designed as a voltage controller, rather than charge based.

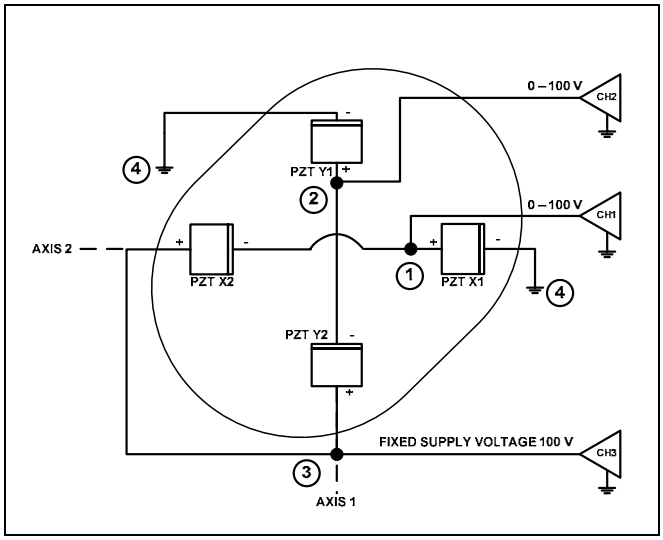

Figure 25 PZT Electromechanical Conceptual Drawing

Reviewing **Figure 25**, we see that three high voltage signals must be generated. One fixed reference of 100V, and a variable signal (0-100V) for each axis of the mirror. The output of the PI with Feedforward controller is limited to op-amp levels. To obtain the high voltage necessary to drive the mirror, a power amplifier was selected and properly scaled for 0 to 100V operation for each axis. Given that the PZT load is primarily capacitive and the signals must travel down a long cable adding more capacitance, the power amplifier selected tolerates highly capacitive loads.

5.6 Controller Overview

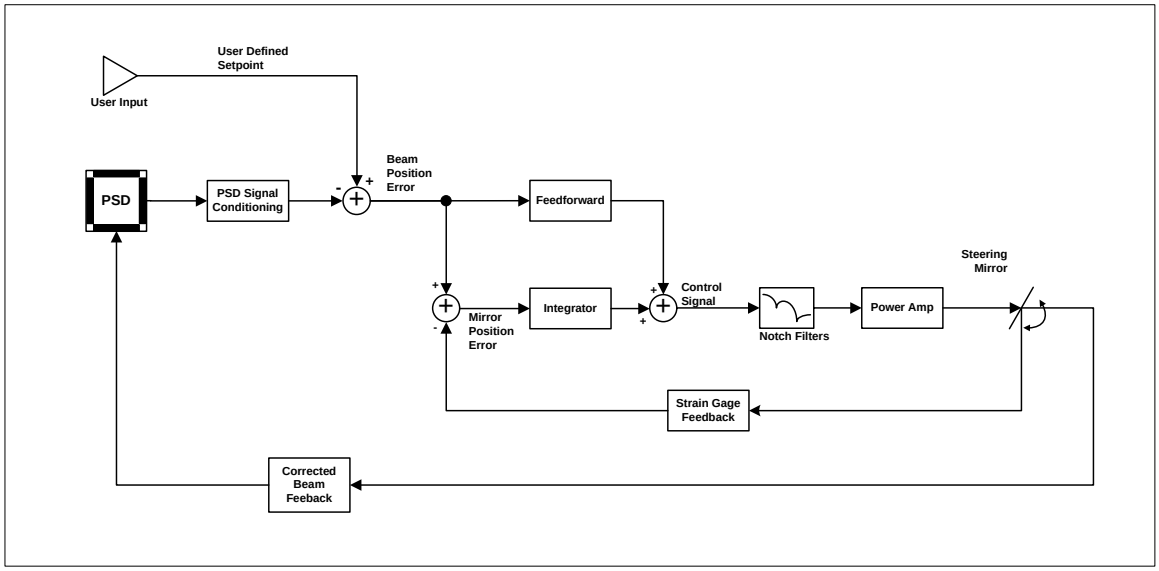

Figure 26 Nested Controller Design Diagram

What emerges from all of this is an analog based nested controller. The front end depends on a PSD to monitor the incoming light. Transimpedance amplifiers convert the PSD generated currents into voltages. These voltages are both added together and subtracted from one another before dividing the difference by the sum to ascertain the position of the incoming beam relative to the center of the PSD. The PSD signal is summed with a user-defined offset to become the active setpoint. The PI with Feedforward controller feeds the setpoint signal forward, as well as passes it to an integrator which compares the setpoint signal with a position signal generated from a scaled strain gauge bridge attached to the mirror. Steady state error is tackled by the integrator. The output of the integrator and the setpoint are summed together and passed through two notch filters. These filtered control signals are scaled to the proper levels to drive the PZTs in the mirror by a power amplifier. When the signals reach the PZTs the mirror moves, causing the location of the incoming beam to shift, and the position signal

generated by the strain gauge bridges to change. The changes in the signals propagate back through the front end and the controller to obtain precise control of the steering mirror. **Figure 26** shows the complete controller design.

6 Closed Loop Performance Analysis

The goals of the project are quire simple: build a steering mirror controller that will operate over temperature, achieve a bandwidth of more than 200 Hz, and a pointing accuracy of 0.08% (40 µrad). The following chapter compares project goals with experimental results to evaluate performance.

6.1 Pointing Accuracy

The ultimate performance metric examines the accuracy of the system. To measure this, the steering mirror control system is operated closed loop and commanded to hold the mirror steady. Examining the power spectral density of the signal generated by the strain gauge amplifier, **Figure 27**, yields system stability.

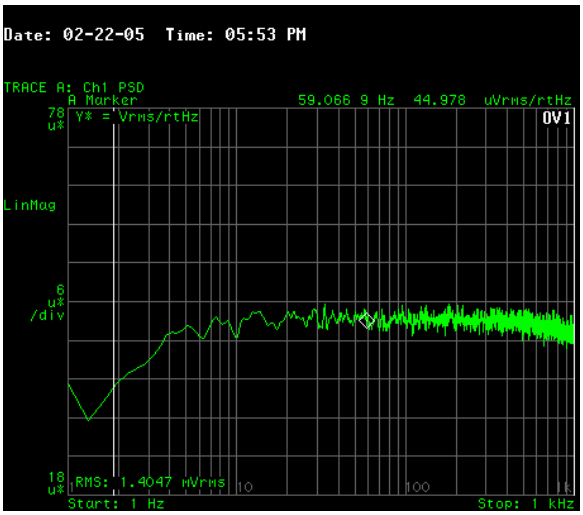

Figure 27 Measured System Power Spectral Density with PI with Feedforward Controller in Closed Loop Operation

The observed Voltage Spectral Density is 1.4 mV_{rms} over a 1kHz bandwidth. The following calculations break the observation down to pointing accuracy.

$$\underline{\underline{Control\ Voltage\ Jitter}} = Strain\ Gauge\ Voltage\ Spectral\ Density \times Circuit\ Gain$$

$$= \left(1.4 \times 10^{-3}\, V\right) \times \left(60 \frac{V}{V}\right)$$

$$= \underline{\underline{0.084V}}$$

$$\underline{\underline{Mechanical\ Jitter}} = Control\ Voltage\ Jitter \times \left(\frac{Motion\ Range}{Control\ Voltage\ Range}\right)$$

$$= 0.084V \times \left(\frac{50{,}000\ \mu rad}{100V}\right)$$

$$= \underline{\underline{42\ \mu rad}}$$

$$\underline{\underline{Percent\ Accuracy}} = \left(\frac{Mechanical\ Jitter}{Motion\ Range}\right) \times 100\%$$

$$= \left(\frac{42\ \mu rad}{50{,}000\ \mu rad}\right) \times 100\%$$

$$= \underline{\underline{0.084\%}}$$

The goal of the design was to achieve and accuracy of 0.08% or 40 µrad. With a strain gauge bridge to control output circuit gain of 60 and 50,000 µrad range, this value amounts to a mirror stability of 42 µrad, or 0.084%. The achieved accuracy is within 0.004% of the design goal.

6.2 Bandwidth

As previously mentioned, project management is primarily concerned with bandwidth as performance measurement. The typical 3dB point is one parameter used to determine bandwidth. The 45° phase shift point is also used as a parameter for bandwidth, due to phase contribution concerns for the overall control system. **Figures 28a** and **28b** show the system response for several controllers.

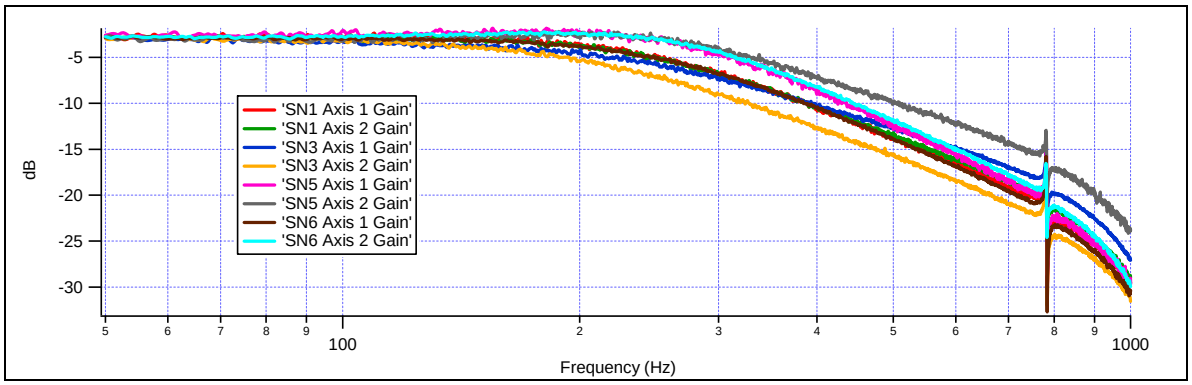

Figure 28a Magnitude Response of 4 Amplifiers over Bandwidth of Interest

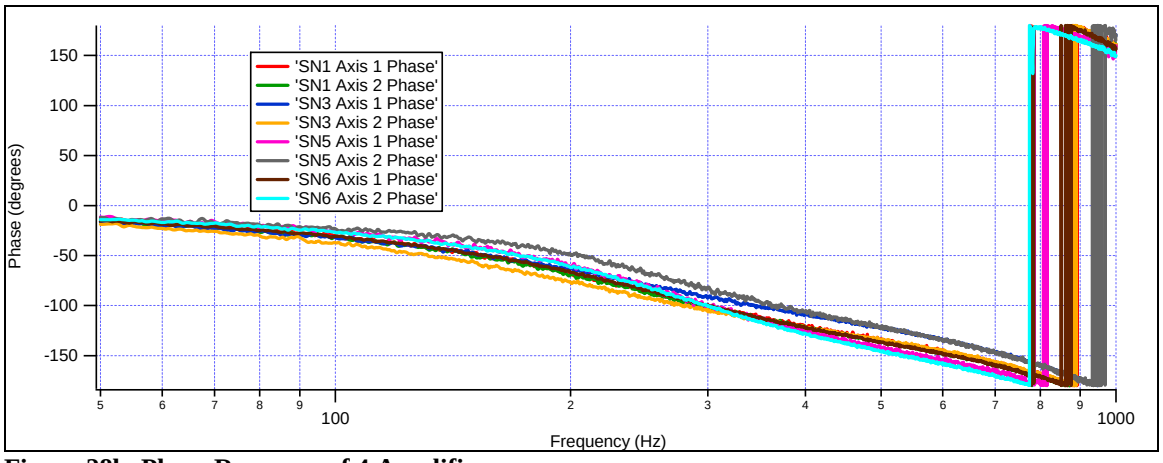

Figure 28b Phase Response of 4 Amplifiers

The average 3dB point for the amplifiers shown is located at roughly 200 Hz, close to the design goal of the controller. However, 45º phase shift occurs at 175 Hz.

Although close to the design goal of 200 Hz, it does fall short. It was expected that the notch filters' affect in the magnitude response would limit the bandwidth. The resulting phase shift from the notch filters has a greater affect and is the limiting term on the bandwidth. In designing an amplifier that could accommodate any mirror, the phase shift resulting from the wide notches is limiting the bandwidth.

In future design iterations, changes in design choices could increase bandwidth. The simplest solution is to incorporate tunable filters which allow for increased bandwidth by shifting the 45^{o} phase shift out further. Each controller would then have to be calibrated to a specific mirror. Different controller topologies may be another avenue to increased bandwidth. Vehedipour and Bobis proposed that a Pseudo-Derivative Feedback (PDF) controller offers faster response and recovery from disturbances than the PID control[8]. The PDF controller places the integral term in the forward loop, and the proportional and derivative terms in the feedback loop. Steady state error is handled by the integrator in the forward loop, while the derivative term in the feedback loop is used to weight the system responsiveness to disturbance[9].

6.3 Time Domain Metrics

Project management is primarily concerned with swift response to disturbances. Consequently, much of this thesis concentrates on bandwidth. However, a glimpse into the time domain response measured at the strain gauge bridge amplifier output gives an indication of how the mirror is physically behaving.

Typical metrics in the time domain are the rise time, peak time, settling time, and percent overshoot.[10] Rise time is defined as the time that it takes the system to rise from 10% to 90% of its final value. This is also an indication of how swiftly the system

responds to disturbances. Peak time, similarly, is defined as the elapsed time for the system to rise from 0% to its peak value. Further, settling time is described as the elapsed time for the system to settle to within a certain percent of it final value, typically 2%. And finally, percent overshoot is defined as the percent difference between the observed peak value and final value of the system.

To obtain the time domain response metrics described above, a 25% of full scale step is applied to the input. The resulting closed loop step response is illustrated in **Figure 29**.

Step Response Metrics

Rise Time = $\boldsymbol{T_r}$ = 1 ms
Peak Time = $\boldsymbol{T_p}$ = 1.5 ms
Settling Time = $\boldsymbol{T_s}$ = 5 ms
Percent Overshoot = **%OS** = 16.6%

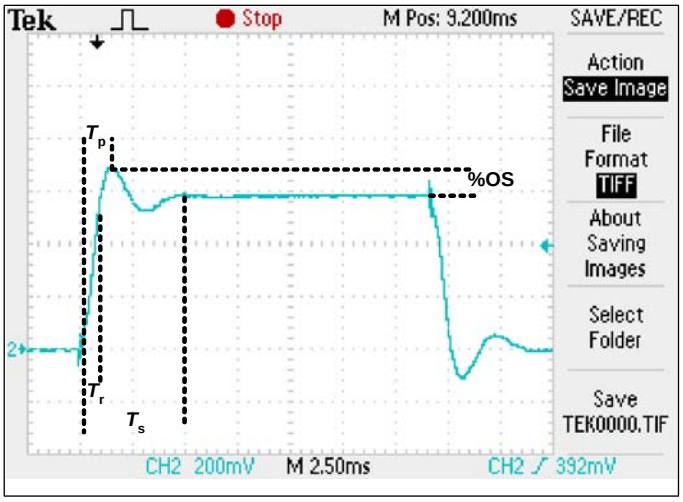

Figure 29 Strain Gauge Step Response

As is typical in controls engineering, decisions in tradeoffs were made to determine acceptable performance. As mentioned previously, project management is primarily interested in bandwidth as the performance metric. The interest in bandwidth is the desire for quick response to disturbances or setpoints. In the time domain, the metric of interest is rise time. The observed 16% overshoot of the system is deemed acceptable given the 1ms rise time observed.

6.4 Performance Limitations

6.4.1 System Resonance and Notch Filter Performance

Concern over exciting the plant at its resonances prompted the use of dual notch filters with tolerances wide enough to handle any mirror. As discussed earlier the use of historical data and computer simulation was used to select a center frequency and Q factor that could accommodate all scenarios. The goal of the filters was to ensure the magnitude response did not surpass unity gain at any point around those resonances. **Figures 30 and 31** below compare simulations to measurements.

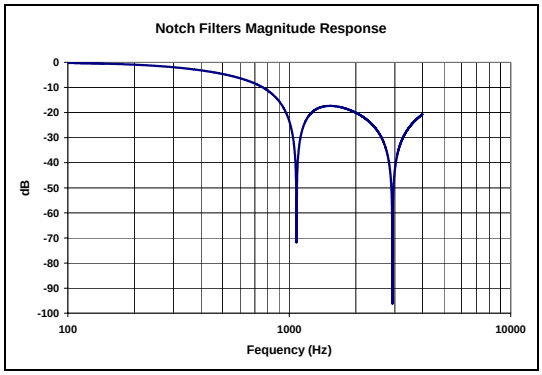

Figure 30(a) Simulated Reponse of Notch Filters

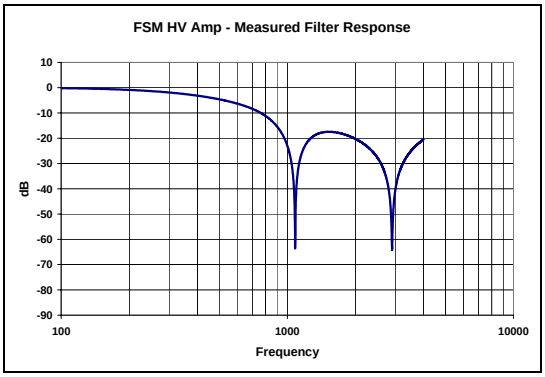

Figure 30(b) Measured Notch Filter Response

In examining the above figures, the measured response performs very closely to the simulated response. The notches do not pull the response quite as low as simulated. The true test of the filters is to examine the system response and ensure that unity gain is not surpassed around the resonances.

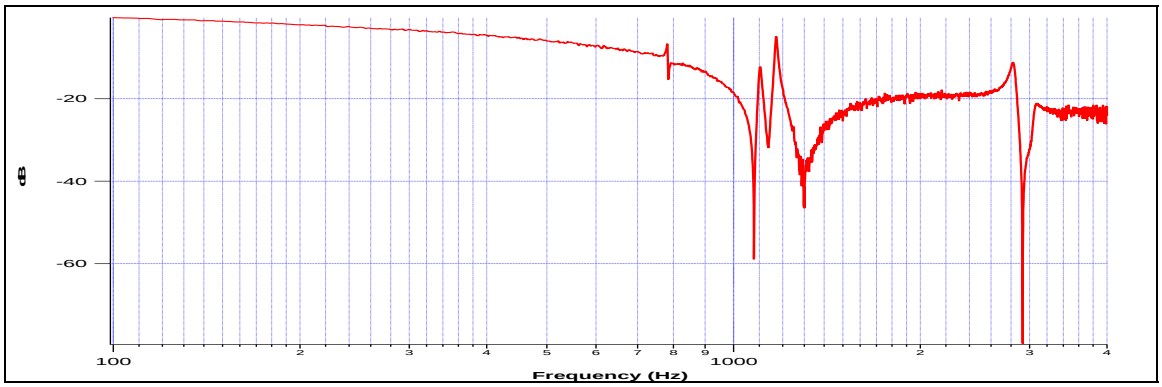

Figure 31(a) Simulated Magnitude Response of Mirror with Notch Filters

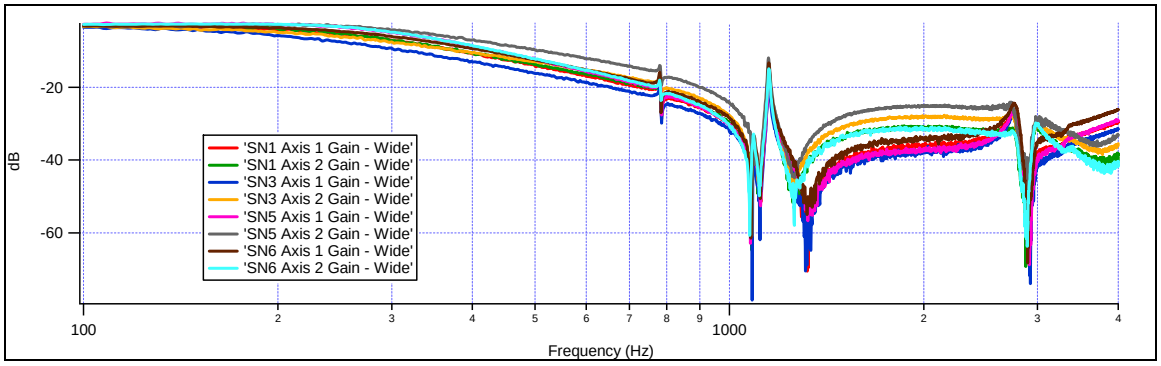

Figure 31(b) Measured Magnitude Response of Mirror Operated by Four Amplifiers

Figure 31(a) graphs the simulated response of the mirror with the filter designed. The measured responses of **Figure 31b** shows the response of each axis of four distinct controllers built. Differences in the observed response can be attributed to slight differences in resistor and capacitor values. At no point does the response cross over into positive gain, thus verifying that the notch filters effectively counteracted the natural resonance of the mirror.

6.4.2 PSD Limitations Due to Low Beam Power

The sensor selected can be a limiting factor in the performance of a system. This is especially true when signal strength degrades. The PSD becomes such a case as light intensity drops. **Figure 32** shows the affects of reducing optical power on the PSD and

the subsequent position error calculated by the analog divider. When the beam power is below 1μW the error grows substantially. The results point to a lower limit of detectability problem.

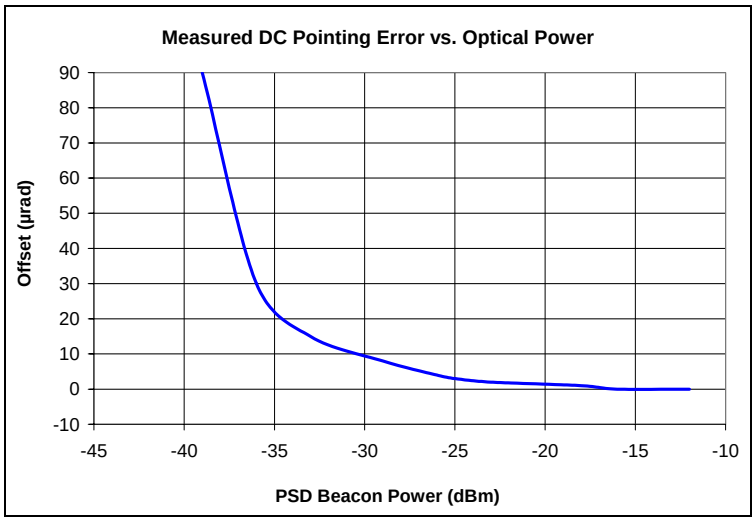

Figure 32 PSD/Divider Power Induced Error

Recalling the equation to calculate position:

$$Beam\ Position = \left(\frac{Length\ of\ PSD}{2}\right)\left(\frac{(Current\ from\ Electrode\ 2 - Current\ from\ Electrode\ 1)}{(Current\ from\ Electrode\ 2 + Current\ from\ Electrode\ 1)}\right)$$

$$= \left(\frac{L}{2}\right) \times \frac{(I_{x2} - I_{x1})}{(I_{x2} + I_{x1})}$$

$$as\ I_{x1}\ and\ I_{x2}\ approach\ zero,$$

$$Beam\ Position = \left(\frac{L}{2}\right) \times \frac{(0)}{(0)} = \infty$$

The denominator of the equation will cause the solution to approach infinity as signal intensity approaches zero. This proves to be a significant error in position resolution.

Obviously boosting the laser power could help, but the particular application of this system restricts power limits of the beam. The use of automatic gain control techniques may also help combat this problem.

7 Conclusions and Future Design Concepts

To reiterate the stated goals at the beginning of this chapter, the goals of the project are quire simple: build a steering mirror controller that will operate over temperature, achieve a bandwidth of more than 200 Hz, and a pointing accuracy of 0.08% (40 µrad). All components are specified by the manufacturer to operate under conditions that meet or exceed -40°C to +80°C, the intended operating range is +25°C to +80°C. The intent of the low Q notch filters was to make controller usable with any mirror. The measured response of the filtered system revealed the resonances never surpassed unity gain, although the phase shift of the filters had detrimental affects on bandwidth. The 3dB bandwidth matched the design goal of 200 Hz; however the 45° phase shift pulls the bandwidth closer to 175 Hz. From a time domain perspective, the closed loop system exhibited a 1ms rise time, 1.5ms peak time, 16.6% overshoot, and 5ms settling time. The measured pointing accuracy of 42 µrad (0.084%) came very close to the design goal of 40 µrad.

Although several goals were achieved with the present design, several changes can be made to improve performance. A significant improvement is to develop a solid model of the system that can be used to tailor a controller to. **Appendix A** shows some preliminary work in this direction. An accurate plant model allows for transitioning to a digital controller. The observed excessive phase shift due to low Q notch filters is limiting the bandwidth of the system. Incorporating the ability to tune the filters for a higher Q calibrated to each individual mirror is one simple improvement that could be implemented that could significantly affect the bandwidth. The discovery of low signal strength affecting position resolution calculations points to giving the PSD particular

scrutiny. Employing Automatic Gain Control (AGC) techniques may help to counteract the effects of signal attenuation through the atmosphere.

Experts in the field have offered a number of suggestions to improve performance. The higher order resonance observed is very similar to the parallel and series resonances of quartz oscillators. Research in this area may yield information in regards to control of such response. The topic of actively dithering the beam during transmission has been discussed as a method to improve signal detectability. Transition to a digital controller has also been suggested as a method to improved performance. The initial work shown in **Appendix A,** as well as the aforementioned topic of tunable filters, lend themselves quite well to digital controllers.

8 Bibliography

[1] Hamamatsu Corp., *PSD: Position Sensitive Detector*, Selection Guide, Hamamatsu City, Japan, July 2003.

[2] Song, Zhao, De Abreau-García, *Tracking Control of a Piezoceramic Actuator with Hysteresis Compensation Using Inverse Preisach Model*, IEEE/ASME Transactions On Mechatronics, Vol. 10, No. 2, April 2005.

[3] Goldfarb, Michael, and Celanovic, Nikola, *Modeling Piezoelectric Stack Actuators for Control of Micromanipulation*, IEEE International Conference on Robotics and Automation, April 1996.

[4] Adriaens, Koning, and Banning, *Modeling Piezoelectric Actuators*, IEEE/ASME Transactions on Mechatronics, Vol. 5, No. 4, December 2000.

[5] Beckwith, Thomas G. and Roy D. Marangoni, *Mechanical Measurements*, Reading, MA, Addison-Wesley Publishing Co., 1990

[6] Williams, Jim, *Bridge Circuits: Marrying Gain and Balance*, Linear Technology Application Note 43, Jun 1990.

[7] Franco, Sergio, *Design with Operational Amplifiers and Analog Integrated Circuits*, San Francisco, CA, McGraw-Hill, Inc., 1988.

[8] Vehedipour, Abbas and James P. Bobis, *Smart Autopilots*, IEEE, 1992.

[9] Parasekevopoulos, Paraskevas N. and George D. Pasgianos,, and Kostas G. Arvanitis, *New Tuning and Identification Methods for Unstable First Order Plus Dead-Time Processes Based on Pseudoderivative Feedback Control*, IEEE Transactions on Control Systems Technology, Vol. 12, No. 3, May 2004.

[10] Dorf, Richard C. and Robert H. Bishop, *Modern Control Systems, 7th Ed.*, Reading , MA, Addison-Wesley Publishing, 1995

Appendix A: Plant Model

The analog controller performs the desired task to the desired specifications, as discussed in Chapter 6. However, recognizing the observed hysteresis in the PZTs and high Q resonance at the mirror's natural frequency and its harmonics are both non-linear behaviours, the analog solution has an obvious shortcoming: it is a linear solution to a non-linear problem.

Development of a solid plant model aids in the design of a digital controller that can address the non-linearities of the mirror. The following chapter discusses the work performed in this area.

A.1 Plant Model Derivation

LabVIEW's System Identification Tool is employed to aid in modeling the plant. The tool analyzes input and output signals for the plant under inspection and creates a mathematical model, or transfer function, of the plant based on that data and parameters such as system order and system type.

To model the steering mirror, a 30% full scale square wave was fed into the mirror operating in an open-loop configuration. This generates a multiple step input and a rich data environment with several frequency components embedded in the strain gauge response. The open loop response is measured to ensure that the model only factors in elements of the plant, and not the controller.

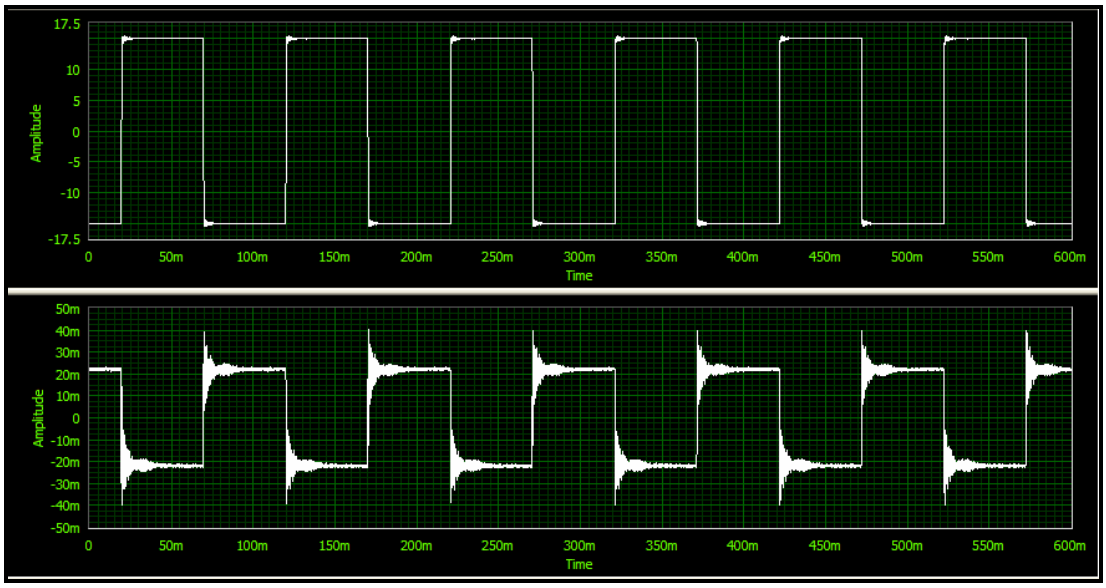

Figure A1 Input/Output Signals for Modeling Tools

The signals displayed in **Figure A1** are the scaled input and output signals used to develop the model. Both input and output data are digitized at 25 kHz and loaded into the software tool.

Parametric Model Estimation methods are applied to the Ouput-Error Model as described by the software documentation[i]. The Output-Error Model is selected because it avoids modeling disturbance signals. An iterative approach is used to determine system order. An 8^{th} order model most closely resembles the previously observed response of the steering mirror. The Bode plot in **Figure A2** shows the resulting model's frequency response. When compared to the measured Bode plot of the steering mirror (**Figure A3)**, the model appears to be a good approximation of the mirror.

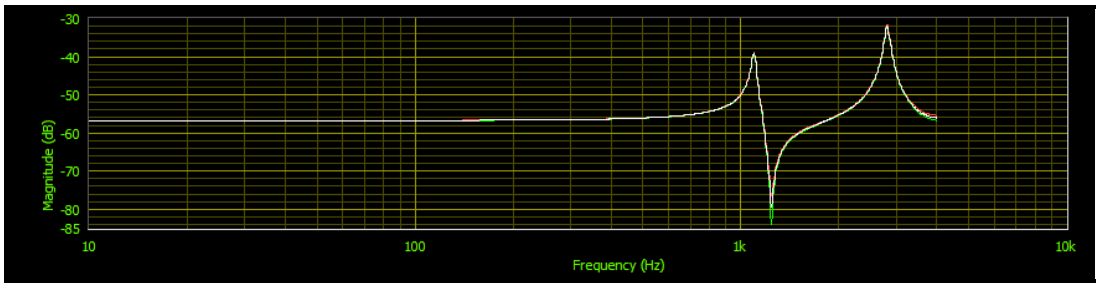

Figure A2 Resulting Bode Plot of Model

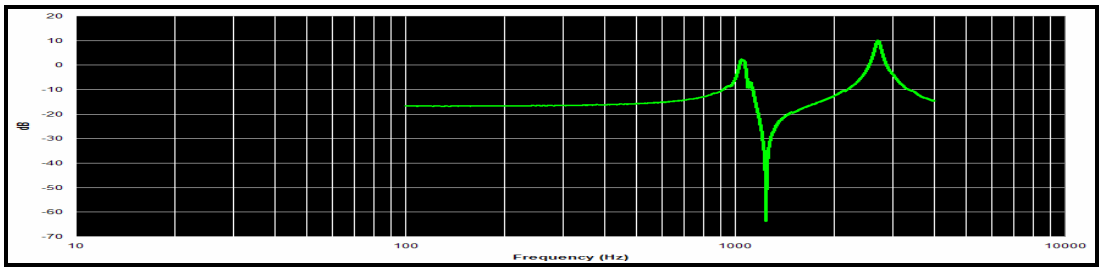

FigureA3 Measured Frequency Response of Mirror

The resulting transfer function defining the steering mirror:

$$T(z)=\frac{-0.00406z^{-1}+0.0022z^{-2}-0.00796z^{-3}+0.01491z^{-4}-0.01504z^{-5}+0.00819z^{-6}-0.00205z^{-7}}{1+0.34773z^{-1}-0.59261z^{-2}+0.50122z^{-3}-0.28185z^{-4}-0.70338z^{-5}+2.32919z^{-6}-2.49554z^{-7}+z^{-8}}$$

[i] National Instruments, *LabVIEW System Identification Toolkit User Manual*, Austin, Texas, September, 2004.

Appendix B: Comparison to Manufacturer Controller

A detail briefly mentioned in the thesis documentation is that this project commenced to replace a manufacturer supplied controller. Although the mirror manufacturer's controller performed as necessary, a few of the features are undesirable for the intended operating conditions and requirements. Among the issues to be addressed are bandwidth, operation over temperature, power consumption, form factor, and weight. **Figure B1** shows the manufacturer's controller. **Figure B2** shows the Lawrence Livermore National Laboratory (LLNL) built controller. **Table B1** makes a brief comparison between the designed controller and the manufacturer controller.

Figure B1 Image of Mirror Manufacturer Controller

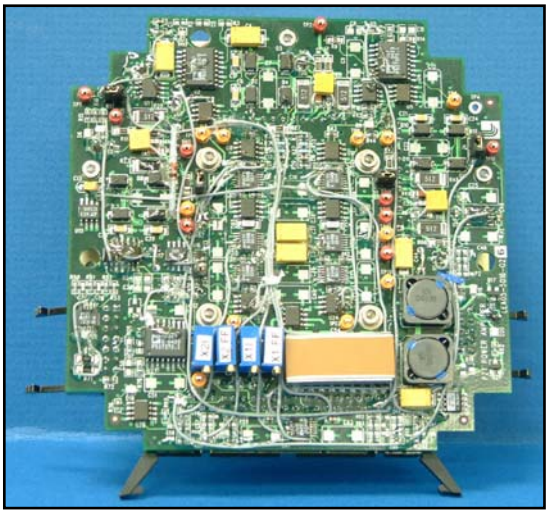

Figure B2a LLNL Built Controller

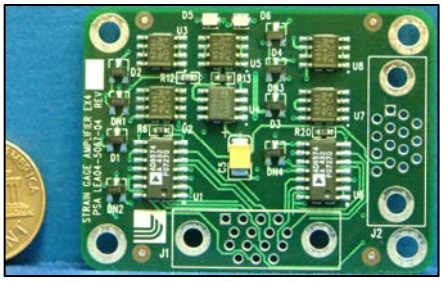

Figure B2b LLNL Built Strain Gauge Bridge Amplifier

Table B1 Design vs. Manufacturer Comparison

Specification	Requirement	Mfr.	LLNL	Improvement
Volume (in^3)	(Not Specified)	655	42	15:1
Weight (gm)	(Not Specified)	6529	618	10:1
Power (W)	(Not Specified)	46	15	3:1
Supply Voltage	28 Vdc	120 Vac	18-36 Vdc	Satisfies Requirement
Temp Range, °C	-20 to +35	25C	-40 to +80	Satisfies Requirement
Bandwidth (Hz)	200 Hz	75	175	1:2.3

Appendix C: Experimental Optical Testbed

An optical testbed was built to verify closed loop operation of the control system. The beam path for the testbed measured 50 inches. Following extensive troubleshooting and calibration, the controller was employed over a 28 km link. Operation was excellent over the long distance link, when atmospheric conditions also were excellent. As mentioned in the text, and displayed in **Figure 32**, the dynamic range in amplitude of the incoming signal limited operation of the control system when atmospheric conditions were poor. **Figure C1** below shows the experimental testbed used under laboratory conditions.

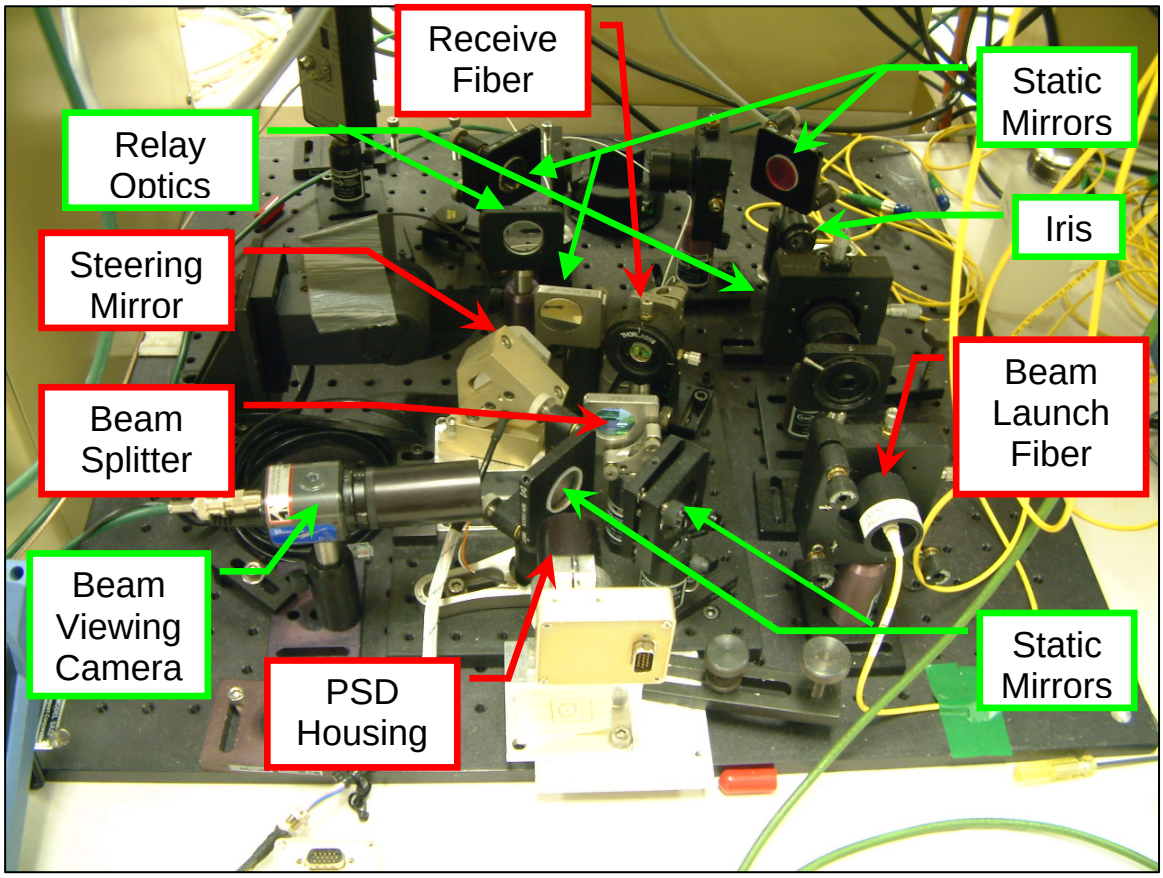

Figure C1 Experimental Optical Testbed